RESEARCH ARTICLE

WILEY

Multi-porous extension of anisotropic poroelasticity: Consolidation and related coefficients

Filip P. Adamus[1] 　│　**David Healy**[2] 　│　**Philip G. Meredith**[1] 　│　**Thomas M. Mitchell**[1] 　│　**Ashley Stanton-Yonge**[1]

[1]Department of Earth Sciences, University College London, London, UK

[2]School of Geosciences, University of Aberdeen, Aberdeen, UK

Correspondence
Filip P. Adamus, Department of Earth Sciences, University College London, London, UK.
Email: adamusfp@gmail.com

Abstract

We propose the generalization of the anisotropic poroelasticity theory. At a large scale, a medium is viewed as quasi-static, which is the original assumption of Biot. At a smaller scale, we distinguish different sets of pores or fractures that are characterized by various fluid pressures, which is the original poroelastic extension of Aifantis. In consequence, both instantaneous and time-dependent deformation lead to fluid content variations that are different in each set. We present the equations for such phenomena, where the anisotropic properties of both the solid matrix and pore sets are assumed. Novel poroelastic coefficients that relate solid and fluid phases in our extension are proposed, and their physical meaning is determined. To demonstrate the utility of our equations and emphasize the meaning of new coefficients, we perform numerical simulations of a triple-porosity consolidation. These simulations reveal positive pore pressure transients in the drained behaviour of weakly connected pore sets, and these may result in the mechanical weakening of the material.

KEYWORDS
anisotropy, fractures, multiple-permeability, multiple-porosity, poroelasticity, rock mechanics

1　│　INTRODUCTION

The deformation of a porous medium containing fluids can be described using equations proposed by Maurice Anthony Biot; an applied physicist born in Belgium. His phenomenological theory relates strains of a solid phase with displacements of fluids. A medium is viewed at a macroscopic, bulk scale, where all pores are treated as interconnected. Constant fluid pressure throughout the medium and a unique measure of the fluid content change is adopted. His theory of three-dimensional consolidation describes time-dependent deformation. It assumes quasi-static stress conditions, incompressible fluid, and flow obeying Darcy's law. In 1935, the isotropic version of consolidation was formulated by Biot in French. Six years later, the more rigorous treatment was written in English.[1] Finally, Biot discussed a more general process of anisotropic consolidation.[2] The developments from the aforementioned papers formulate the core of the so-called (quasi-static) poroelasticity. The quasi-static approach will also be considered in this paper.

Since the publication of the original theory of poroelastic consolidation, some generalizations were proposed. Biot[3] considered a viscoelastic extension. Further, Biot[4] formulated the finite elastic description of porous structures. Other researchers introduced more modifications. Booker and Savvidou[5] generalized the consolidation equations by including a thermal stress term. Chemical effects were considered by Sherwood.[6] Various impacts were combined to provide multi-physical formulations for porous materials by Taron et al.[7] They linked the usual mechanical and hydraulic poroelastic coupling with thermal and chemical effects. Note that all the above extensions go beyond the theory of poroelasticity. These generalizations constitute foundations of the theories of *finite poroelasticity*, *porothermoelasticity*, *porochemoelasticity*, or *porothermochemoelasticity*, respectively [8, Chapter 12]. In this paper, however, we do not go beyond poroelasticity. Instead, we consider an extension within the frame of elastic, mechanical-hydraulic coupling.

Such an extension within Biot's poroelastic frame was first formulated by Aifantis,[9–12] a physicist born in Greece. His generalization of consolidation equations was based on the idea of the so-called dual or multiple-porosity. In this paper, terms using notion of porosity describe a pore space instead of referring to a scalar quantity describing the volume fraction occupied by voids. Therefore, we define a "multi-porous" medium (the original nomenclature of Aifantis) or a material with multiple-porosity (common nomenclature in literature) as a structure that consists of two or more pore sets that are characterized by different fluid pressures and diffusions. Therein, each set consists of a system of connected pores that are defined as empty or saturated voids having any shape, including microcracks or fractures. Hence, the assumption of uniform fluid pressure in all pores, originally introduced by Biot, is removed. It is important to mention that the concept of spatially varying pressure has been known long before the aforementioned works. Barenblatt et al.[13] were the first to introduce the dual-porosity approach and Warren and Root[14] were the first to discuss its use in practice. However, these authors considered the problem of fluid diffusion only. As noticed by Elsworth and Bai,[15] until the work of Aifantis,[9] the hydrologic description was not coupled with mechanics since the stresses were assumed to be constant.[16,17] In the classical dual-porosity analysis of fluid diffusion, the fractures and solid matrix contribute to the overall behaviour in distinctly different ways due to decidedly different characteristics; the fractures commonly have high permeability and low storativity, whereas the solid matrix tends to have the opposite characteristics. Therefore, it is reasonable to expect the poromechanical contributions of the fractures to vary from that of the solid matrix. The works by Aifantis led to the multi-porous extension of the isotropic poroelasticity theory. The aim of this paper is to generalize the formulations of Aifantis by considering the effect of anisotropy caused by the structure of the solid matrix and different sets of pores.

Since the pioneering work of Aifantis,[9] the multi-porous (including dual-porosity) consolidation was discussed continuously by numerous researchers for over 40 years (see, revision of Ashworth and Doster[18]). First, Wilson and Aifantis[19] determined the extended poroelastic coefficients in terms of volume fractions and various bulk moduli. Then, Khaled et al.[20] formulated the consolidation equations using coefficients of fluid content change utilized by Biot. Cho et al.[21] introduced anisotropy to the solid skeleton and one type of porosity; however, the poroelastic coefficients still remained isotropic. Berryman and Wang[22] proposed a novel representation of isotropic strain-stress relations, linked with symmetric coefficients a_{ij}. They discussed the physical meaning of each coefficient. The alternative determination using the so-called uniform expansion thought experiment was discussed by Berryman and Pride[23] and Berryman.[24] Further, Nguyen and Abousleiman[25] and Mehrabian and Abousleiman[26] solved isotropic Mandel-type consolidation problems. The latter work provided explicit formulations for multi-porous consolidations. Mehrabian[27] discussed isotropic strain-stress, stress-strain, and mixture relations in view of the multi-porous coefficients. Recently, Zhang and Borja,[28] Zhao and Borja,[29] and Zhang et al.[30] provided an anisotropic extension of the dual-porosity diffusion equation using stress-strain relations and various non-phenomenological methods that did not include Biot's fluid increment coefficient, ζ. In this paper, our novel extension is based on Biot's approach, where the fluid continuity equations[1] are used. We present new derivation of anisotropic equations of multi-porous three-dimensional consolidation that origins from the works of Biot, Aifantis, and Berryman. Both methodology and notation is analogous to their works. Note that our derivation differs from alternative solutions of Zhang et al.[31] and Zhang and Mehrabian[32] who base their derivations on thermodynamics and operate with alternative coefficients. Also, our anisotropic poroelastic coefficients differ from the ones of Zhang and Borja[28] since our coefficients are derived from strain-stress relations without the assumption of superposition. Part of our physical determination methodology is similar to that of Berryman and Wang.[22]

Before we move to the theoretical derivations (Sections 3–6) followed by numerical examples (Section 7), we first sketch in the next section the idea of our anisotropic multi-porous extension and indicate its potential usage. Also, we refer to previous works that considered the practical aspects of dual porosity. Although we focus on the porous structures present in rocks, analogous analysis may be performed in the context of other poroelastically behaving media (e.g., bones).
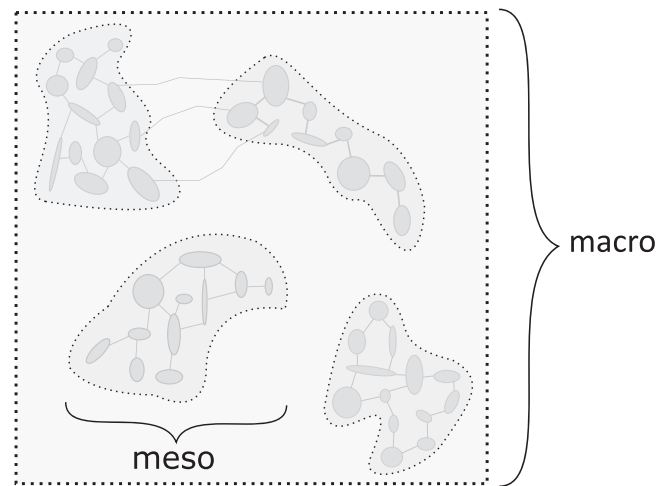
FIGURE 1 Schematic view of the multi-porous extension that considers a quasi-static medium at a macroscopic scale and distinguishes pore sets at a mesoscopic scale. Sets are allowed to be weakly connected (see upper part).

2 | POTENTIAL USAGE OF ANISOTROPIC MULTI-POROUS EXTENSION

Many porous materials, such as rocks, composites, or human tissues, exhibit anisotropic behaviour. The directional-dependent mechanical response of a medium can have various causes that are often combined. The anisotropy may be intrinsic (e.g., arrangement of crystals), induced by inhomogeneities (e.g., pores), or induced by stress (e.g., fractures that record deformation due to pre-existing loads). As mentioned in the previous section, we allow the two former origins of anisotropy in porous media. The intrinsic anisotropy is described by a solid matrix. If pores are not spherical and are not randomly oriented, then induced anisotropy is additionally present.

2.1 | Levels of connectivity: Spatial variations

Certain anisotropic materials possess multiple pore sets, meaning that a medium contains voids that are well connected within particular sets but sets themselves are either weakly connected or isolated at any given time. Then, our multi-porous extension of anisotropic poroelasticity theory can be used to describe the mechanics of such media, where the level of connectivity between pores affects fluid diffusion and leads to pressure variations. Although the original Biot theory has a macroscopic nature (quasi-static assumption), in our extension, the mesoscale structures are also distinguished (different pore sets), as schematically depicted in Figure 1. Further, one can also search for the micromechanical link to the theory (pore geometry); such linkage is discussed in our parallel paper.[33] We subjectively distinguish three types of porous structures, where our extension is pertinent: hierarchical porosity, complex porosity, and clustered porosity formed by spatially-distributed pore sets. Each type is presented in Figure 2 and discussed below.

Hierarchical porosity describes a scenario where there are multiple pore sizes in the medium[34] forming a nested structure, like in a Russian matryoshka doll.[35] Such porosity can be found in geomaterials, extended framework materials, foams, fibres, vascular plants, or body tissues. Examples of hierarchically porous rocks involve carbonates during the dolomitization process (Figure 2A) or microporous sandstones having macropores at grain boundaries (Figure 2B). The former consist of microporosity, abundant intercrystalline pores, and some irregular vuggy pores that form during the advanced stage of the dolomitization process.[36] The dolostones are interesting not only from a purely geological perspective (dolomitization) but also from a resource exploration point of view—approximately 50% of the world's gas and oil reservoirs are in carbonate rocks,[37] and many ore deposits are hosted in dolostones.[38] The porosity of clean sandstones is simpler; macroporosity forms a relatively uniform intergranular network, and microporosity forms from detrital and authigenic clays.[39] Sandstones are also important for petroleum geology since they commonly host oil and gas.[40] Biomechanical examples involve bone tissue, tendon tissue, or meniscus tissue; extension of the poroelasticity theory can be used to model the mechanical and blood pressure load-driven movements.[35] Also, synthesis and

ADAMUS ET AL.

(A) Hierarchical porosity: dolostone

(B) Hierarchical porosity: sandstone

(C) Complex porosity: sandstone

(D) Complex porosity: coal

(E) Clustered porosity: sample scale
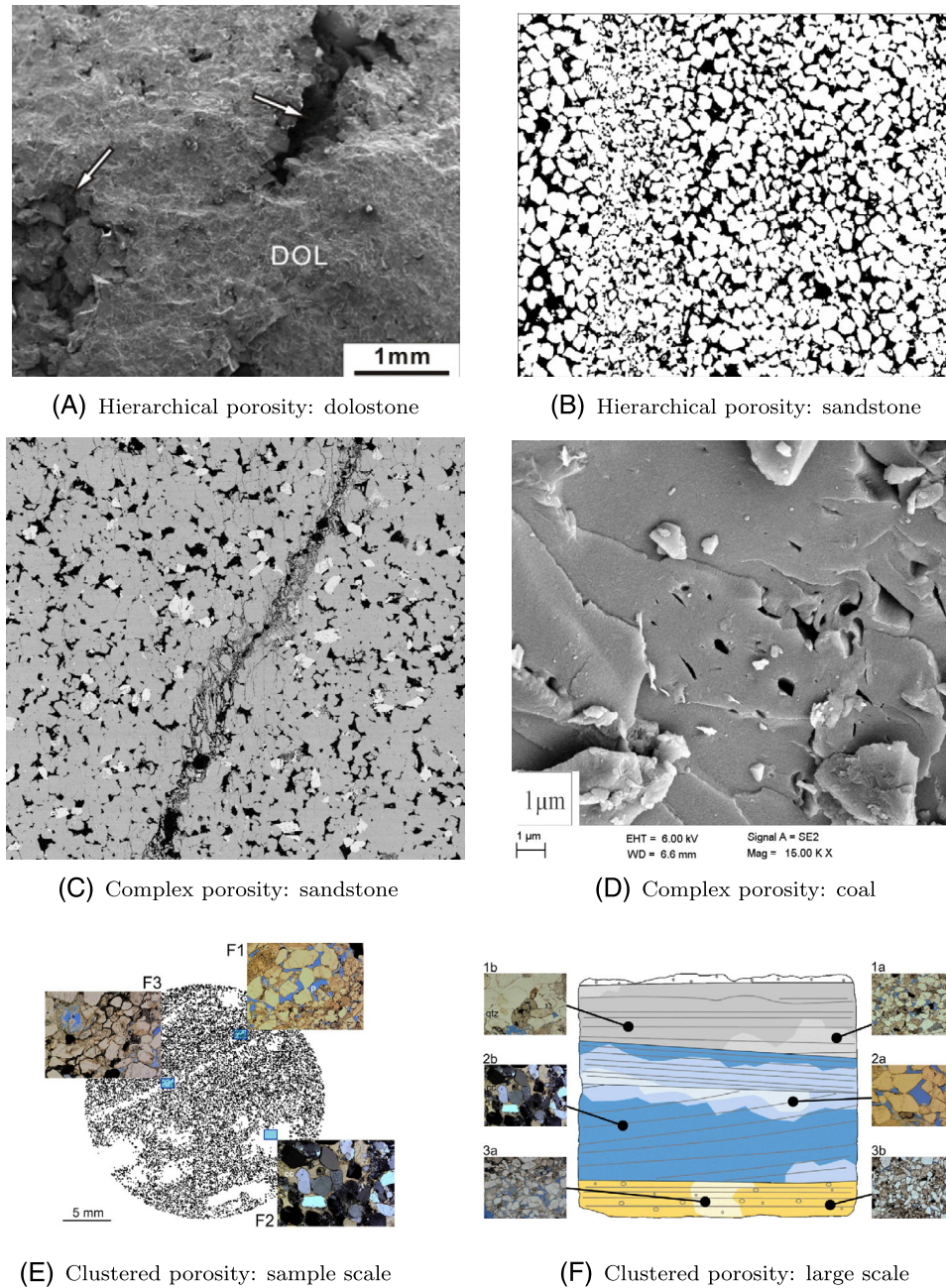
(F) Clustered porosity: large scale

FIGURE 2 Literature examples (granted permissions by corresponding authors) with porosity types pertinent to the multi-porous extension. (A) Dolostone with irregular vuggy pores (arrows) and smaller intercrystalline pores from Wang et al.[36] (B) Porous sandstone with pores of different sizes from Farrell et al.[54] (C) Fractured sandstone with micropores from Rizzo et al.[55] (D) Coal with cleats and micropores from Panwar et al.[56] (E) Sandstone at a sample scale and (F) field scale taken from Heidsiek et al.[52]

applications of hierarchically structured porous materials has become a rapidly evolving field of current interest.[41] The theory of dual porosity was applied to, for instance, perforated concrete[42] and sound-absorbing materials,[43] like foams and fibres.[44]

We refer to a complex porosity where microcracks or larger fractures intersect a medium having background porosity. Such a scenario commonly occurs in geomaterials (e.g., coals, tight-gas sands). Among many fields, the dual-porosity theory is widely applied in petroleum science.[45–47] Originally, the dual-porosity concept was studied to describe the mechanics of conventional fractured reservoirs,[14] represented by for example, fractured porous sandstone (Figure 2C). Also, the extended theory of Biot was used to describe unconventional reservoirs, such as coalbed methane.[48] Coals (Figure 2D) contain natural fractures with different permeability than the porous background.[49] Alternatively, dual porosity can be

applied to a fractured geothermal reservoir,[50] such as hydrothermally altered granite.[51] Note that fractured rocks are usually anisotropic due to the preferred orientation of the fractures and, at a large scale, fracture networks can demonstrate strongly different fluid flow behaviours.[79] Hence, two or more pore sets might need to be considered to describe such phenomena.

We use the term clustered porosity to describe spatially-distributed pore sets that form non-overlapping concentrations. In other words, pores (e.g., cracks) having fixed poroelastic constants are not dispersed throughout the medium, but they constitute a set that is spatially separated from pores having different characteristics (see Figure 1). For instance, Heidsiek et al.[52] examine a reservoir sandstone with pore sets that vary spatially when viewed at both the sample-scale (Figure 4A) and the grid-cell scale relevant to reservoir studies (Figure 4B). Brantut and Aben[53] measured local fluid-pressure variations within laboratory-scale samples of sandstone and granite. At a large field scale, pore sets and permeabilities also vary spatially. However, to use the multi-porous extension, the considered medium cannot be too large since the solid-matrix stiffness must be uniform, and quasi-static assumptions must be obeyed. To evaluate large spatial domains, like reservoirs, a discretization into smaller scales may be needed.[46]

Having discussed types of porous structures and indicated studies where the simplified dual-porosity extension has already been applied, we can now list the anisotropic multi-porous extension potential applications. We believe that the aforementioned extension might be successfully applied to structures having:

- hierarchical porosity with more than two gradations (micropores, mesopores, macropores),
- complex porosity with microcracks or fractures allowing preferential flow (background porosity, microcracks, fractures with slow flow, macro-fractures with fast flow),
- clustered porosity formed by more than two spatially-distributed pore sets,
- mixtures of the porosity types listed above (micropores, macropores, fractures or clustered hierarchical porosity or clustered complex porosity).

2.2 | Levels of connectivity: Temporal variations

Combined with the spatial variations that need a multi-porous description, it is also necessary to take into account the temporal variations of pore space and its level of connectivity. Note that in this paper, we do not formally consider the detailed processes of pore nucleation, growth, coalescence and closure within our model, but we emphasize that these processes will impact the equilibration of fluid pressure in space and time. A simple binary classification into a dual-porosity model of pore space may be insufficient to describe this behaviour. Building on the simple framework of the so-called primary and secondary porosity proposed by Warren and Root,[14] we recognize that after lithification and the incorporation of primary porosity in sedimentary or igneous rocks, many processes lead to changes in the volume fraction of pores. Thus, pores can become more—or less—connected. For example, cracks can grow in response to stress, but at the instance of their opening, they will be empty, and it will take a finite time for them to fill with fluid. Over time, such cracks will coalesce and connect to allow fluid flow (and thereby tend to equilibrate fluid pressure). If the rate of crack growth exceeds the hydraulic diffusivity, then dilatancy hardening will ensue.[57] For low permeability rocks, such as shales, the fraction of total pore space that contributes to fluid pathways can vary with load and fluid pressure. Rutter et al.[58] found that less than 10% of total pore space in shales is 'used' by the flowing fluid during laboratory tests under elevated effective pressure. By contrast, dehydration reactions in metamorphic rocks can produce new, isolated pore space that is fluid-filled from its nucleation. This arises because the pore fluid is a 'new' fluid released locally by the dehydration reaction rather than flowing in from an external source. Even in a two-phase system, such as gypsum and water, dehydration reaction progress and the evolution of porosity and permeability are non-trivial: Leclère et al.[59] detail how the formation of metastable bassanite during the dehydration of gypsum to anhydrite under stress leads to a marked increase in volume fraction of pore space as it is stronger than gypsum and thereby develops a relatively rigid framework which can support the newly formed pores: these pores then grow and connect to create permeability. In addition to these void-creation mechanisms, there are processes that can lead to the loss of pore space and connectivity. For example, localized compaction in initially highly-porous rocks can lead to decreases in volume fraction of pore space and orders of magnitude decreases in permeability.[60] Furthermore, hydration reactions consume pore fluids and lead to the closure and healing of pores. All these dynamic processes are ubiquitous in natural rocks over a wide range of physical conditions, and they lead us to reaffirm the fundamental observation that pores—and the connections between
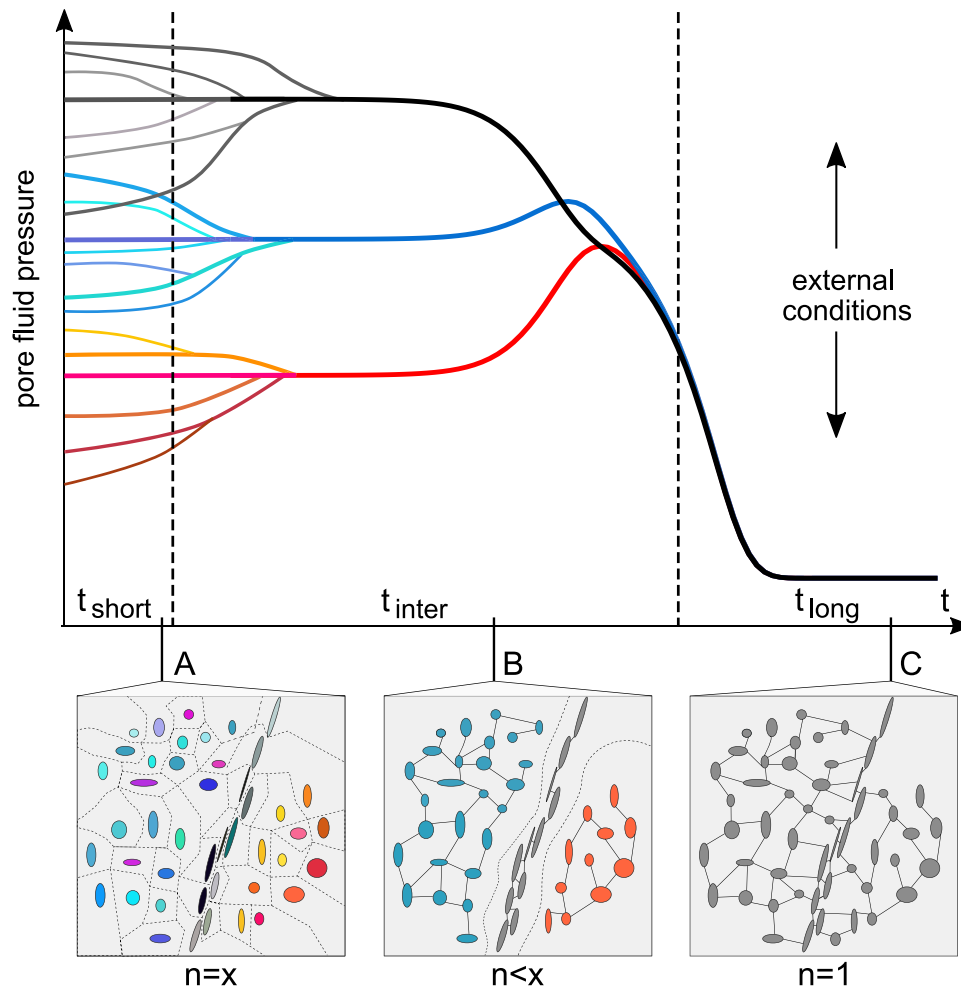
FIGURE 3 Schematic view of the conceptual model with timescale and scenarios described in the main text, where x denotes the number of pores and n stands for the number of pore sets. The drainage leads to the equilibrated fluid pressure; its value depends on the external conditions present.

them—continuously evolve over time (and space). Consequently—at any given instant—some pores (and sets thereof) will be connected, and flow between them is possible, whereas others—at any given instant—will be isolated. The connectivity of pores to reach a percolation threshold for hydraulic flow takes a finite time to achieve and, critically, is not irreversible.

2.3 | Conceptual model

As described above, pores can open or close in response to different mechanisms and driving forces, and critically this produces variations in connectivity. We, therefore, propose a new conceptual model of time-dependent pressure variations in this non-uniformly connected porous medium, which we refer to as a stream-river model (see Figure 3). This model—under given external conditions—progresses towards fully drained (connected) behaviour. At early times, pores are isolated or weakly connected and fluid pressures vary throughout (t_{short}, scenario A). As fluid diffuses and connections develop among pores in a set, the pressure distribution begins to simplify (t_{inter}, scenario B). Eventually, as the system approaches full connectivity and exceeds the percolation threshold, there is a single fluid pressure (t_{long}, scenario C). Hence, as time progresses, the number of sets, n, decreases from $n = x$—where there are x pores being formally equivalent to x sets containing one pore each—towards $n = 1$, which stands for classical poroelasticity. Note that due to a large number of pores at early times, we advise utilizing the model in less complex situations where the connectivities within sets are already established (see Section 7).

This, then, is our rationale for developing a generalized multi-porous extension to the classical theory of anisotropic poroelasticity. Our aim is to produce an analytical solution, rather than a wholly numerical method, in order to be able to explain the physical meaning of the terms involved.

3 | STRAIN-STRESS RELATIONS

Herein, we study the constitutive equations that describe the properties of a deformable elastic medium containing pores. In these equations, the deformation is viewed at a given instant. Strains and fluid content changes are related to the changes in stresses and pore pressures through poroelastic constants. In other words, all discussed variables (like stress, pore pressure, etc.) are viewed as instantaneous changes, rather than as absolute values. The deformation is assumed to be small so that linear relations can be utilized. In this section, the process of material consolidation or swelling is not considered since time dependency is excluded. We should also note that the sign convention here follows that of elasticity; stresses and strains are positive in the tensile direction. A list of nomenclature can be found in the article.

Before we describe the constitutive equations, we should define the strains of the porous medium. The bulk strain tensor,

$$e_{ij} := \frac{1}{2}\left(\frac{\partial u_i}{\partial x_j} + \frac{\partial u_j}{\partial x_i}\right), \tag{1}$$

where u_i are the displacements of a skeleton (solid with empty pores) in the i-th direction; x_i denote the coordinate axes. Throughout the paper, $i, j \in \{1, 2, 3\}$. In the case of isotropic medium and hydrostatic confining pressure, the displacements in the principal directions are equal. Hence, the volumetric strain can be written as $e := \frac{1}{3}\sum_i \partial u_i/\partial x_i = e_{ii}$. The change in the fluid content is more difficult to describe due to the varying nature of material porosity. Let us use a superscript (p), where $p \in \{1, \ldots, n\}$, to denote a specific set in a n-porosity medium. Following Biot,[61] we define

$$\zeta^{(p)} := \phi^{(p)} \sum_{i=1}^{3} \frac{\partial u_i - \partial U_i^{(p)}}{\partial x_i}, \tag{2}$$

where $U_i^{(p)}$ is the displacement of the fluid contained in the p-th pore set; the volume fraction occupied by such a set is denoted by $\phi^{(p)} \equiv V^{(p)}/V$. Expression (2) describes a relative volumetric strain of a fluid with respect to the solid, loosely referred to as "fluid increment" or "fluid content change" of a p-th pore set. Importantly, the fluid content changes between sets are not taken into account yet. In other words, $\zeta^{(p)}$ should be viewed as a quantity that depends on the external behaviour of the bulk medium considered.

First, let us consider the constitutive equations for isotropic single porosity.[1] They relate volumetric strain e and fluid increment $\zeta \equiv \zeta^{(1)}$, to the changes in confining pressure p_c and changes in fluid pressure $p_f \equiv p_f^{(1)}$, through drained bulk modulus K and poroelastic coefficients. Changes in pressure are positive in compression. In the matrix notation,

$$\begin{bmatrix} e \\ -\zeta \end{bmatrix} = \begin{bmatrix} \frac{1}{K} & \frac{1}{3}SB \\ \frac{1}{3}SB & S \end{bmatrix} \begin{bmatrix} -p_c \\ -p_f \end{bmatrix},$$

where S and B are the storage and Skempton coefficients, respectively.

Let us consider the constitutive equations for isotropic dual porosity.[22] Due to the various characteristic of pore sets, fluid content and pressure changes are not constant throughout the medium. The increments $\zeta^{(1)}, \zeta^{(2)}$ are related to the pore pressure changes of the first $p_f^{(1)}$ and second pore set $p_f^{(2)}$ by means of coefficients a_{ij}, namely,

$$\begin{bmatrix} e \\ -\zeta^{(1)} \\ -\zeta^{(2)} \end{bmatrix} = \begin{bmatrix} a_{11} & a_{12} & a_{13} \\ a_{12} & a_{22} & a_{23} \\ a_{13} & a_{23} & a_{33} \end{bmatrix} \begin{bmatrix} -p_c \\ -p_f^{(1)} \\ -p_f^{(2)} \end{bmatrix}. \tag{3}$$

The a_{ij} coefficient matrix must be symmetric because the scalar of the two remaining matrices is the potential energy.[62] The existence of the potential energy function implies the invariance of the coefficient matrix under permutations of

subscripts i and j. The above form was first given by Berryman and Wang[22]; the original sign convention is preserved. We can treat the strains and stresses as tensors—instead of scalars—and represent them as 6×1 vectors. They are related by the elastic compliances $S_{ijk\ell}$. Hence, without changing any assumptions, we can rewrite isotropic relations (3) as

$$
\begin{bmatrix}
e_{11} \\
e_{22} \\
e_{33} \\
0 \\
0 \\
0 \\
-\zeta^{(1)} \\
-\zeta^{(2)}
\end{bmatrix}
=
\begin{bmatrix}
S_{1111} & S_{1122} & S_{1122} & 0 & 0 & 0 & -b^{(1)} & -b^{(2)} \\
S_{1122} & S_{1111} & S_{1122} & 0 & 0 & 0 & -b^{(1)} & -b^{(2)} \\
S_{1122} & S_{1122} & S_{1111} & 0 & 0 & 0 & -b^{(1)} & -b^{(2)} \\
0 & 0 & 0 & S_{2323} & 0 & 0 & 0 & 0 \\
0 & 0 & 0 & 0 & S_{2323} & 0 & 0 & 0 \\
0 & 0 & 0 & 0 & 0 & S_{2323} & 0 & 0 \\
-b^{(1)} & -b^{(1)} & -b^{(1)} & 0 & 0 & 0 & a_{22} & a_{23} \\
-b^{(2)} & -b^{(2)} & -b^{(2)} & 0 & 0 & 0 & a_{23} & a_{33}
\end{bmatrix}
\begin{bmatrix}
\sigma_{11} \\
\sigma_{22} \\
\sigma_{33} \\
0 \\
0 \\
0 \\
-p_f^{(1)} \\
-p_f^{(2)}
\end{bmatrix},
$$

where $S_{1122} = S_{1111} - 2S_{2323}$, $e_{11} = e_{22} = e_{33} = e/3$, and $\sigma_{11} = \sigma_{22} = \sigma_{33} = -p_c$. Coefficient $b^{(1)} =: -a_{12}/3$ and $b^{(2)} =: -a_{13}/3$. This form is analogous to the one shown by Berryman and Wang.[62] Note that pressure changes have the opposite sign to stress changes, σ_{ij}.

The equations for isotropic dual porosity can be translated into a general anisotropic case as follows.

$$
\begin{bmatrix}
e_{11} \\
e_{22} \\
e_{33} \\
e_{23} \\
e_{13} \\
e_{12} \\
\zeta^{(1)} \\
\zeta^{(2)}
\end{bmatrix}
=
\begin{bmatrix}
S_{1111} & S_{1122} & S_{1133} & S_{1123} & S_{1113} & S_{1112} & b_{11}^{(1)} & b_{11}^{(2)} \\
S_{1122} & S_{2222} & S_{2233} & S_{2223} & S_{2213} & S_{2212} & b_{22}^{(1)} & b_{22}^{(2)} \\
S_{1133} & S_{2233} & S_{3333} & S_{3323} & S_{3313} & S_{3312} & b_{33}^{(1)} & b_{33}^{(2)} \\
S_{1123} & S_{2223} & S_{3323} & 2S_{2323} & 2S_{2313} & 2S_{2312} & b_{23}^{(1)} & b_{23}^{(2)} \\
S_{1113} & S_{2213} & S_{3313} & 2S_{2313} & 2S_{1313} & 2S_{1312} & b_{13}^{(1)} & b_{13}^{(2)} \\
S_{1112} & S_{2212} & S_{3312} & 2S_{2312} & 2S_{1312} & 2S_{1212} & b_{12}^{(1)} & b_{12}^{(2)} \\
b_{11}^{(1)} & b_{22}^{(1)} & b_{33}^{(1)} & b_{23}^{(1)} & b_{13}^{(1)} & b_{12}^{(1)} & a_{22} & a_{23} \\
b_{11}^{(2)} & b_{22}^{(2)} & b_{33}^{(2)} & b_{23}^{(2)} & b_{13}^{(2)} & b_{12}^{(2)} & a_{23} & a_{33}
\end{bmatrix}
\begin{bmatrix}
\sigma_{11} \\
\sigma_{22} \\
\sigma_{33} \\
\sigma_{23} \\
\sigma_{13} \\
\sigma_{12} \\
p_f^{(1)} \\
p_f^{(2)}
\end{bmatrix}.
\tag{4}
$$

We see that coefficients $b^{(p)}$ transformed into second-rank tensors, and negative signs have canceled. Factor 2 in front of certain compliances appeared due to the index symmetries of the stress tensor. The meaning of a_{ij} and $b_{ij}^{(p)}$ will be explained in the next section. Straightforwardly, we generalize the above form to the multiple-porosity, n-set scenario, namely,

$$
\begin{bmatrix}
\mathbf{e} \\
\zeta^{(1)} \\
\vdots \\
\zeta^{(n)}
\end{bmatrix}
=
\begin{bmatrix}
\mathbf{S} & \mathbf{b^{(1)}} & \cdots & \mathbf{b^{(n)}} \\
\mathbf{b^{(1)}}^T & a_{2,2} & \cdots & a_{2,n+1} \\
\vdots & \vdots & \ddots & \vdots \\
\mathbf{b^{(n)}}^T & a_{2,n+1} & \cdots & a_{n+1,n+1}
\end{bmatrix}
\begin{bmatrix}
\boldsymbol{\sigma} \\
p_f^{(1)} \\
\vdots \\
p_f^{(n)}
\end{bmatrix},
\tag{5}
$$

where $\mathbf{e}$, $\mathbf{b^{(p)}}$, $\boldsymbol{\sigma}$ are 6×1 vectors, $\mathbf{S}$ is a 6×6 matrix and ^{T} denotes the transposition. In the next sections, we will strive to get more insight into the novel Equations (4)–(5) given above.

4 | DETERMINATION OF a_{ij} AND $b_{ij}^{(p)}$

In their present form, a_{ij} and $b_{ij}^{(p)}$ are difficult to measure in practice, and their physical meaning is unclear. Therefore, in this section, we describe them in terms of elastic compliances and poroelastic coefficients (Skempton-like and storages).

We consider various poroelastic boundary conditions that lead to the a_{ij} and $b_{ij}^{(p)}$ determination. This way, a few universal constraints for weakly-connected sets are also provided.

The standard boundary conditions of poroelasticity are referred to as the drained and undrained states, defined by no change in fluid pressure and no change in fluid content, respectively. Another possible limit is that of constant confining stress, $\boldsymbol{\sigma} = \mathbf{0}$ (this is not an absolute value). Such a condition is strived to be achieved in the fluid injection tests. However, in the case of a multiset extension, more variables require more boundary conditions that need to be considered. Besides, if sets are weakly connected, the long-time limit leads to pressure equilibration. In turn, the constraints for weakly-connected sets can be formulated. Below, we provide idealized scenarios—as a basis for designing suitable laboratory experiments—that provide the aforementioned constraints and useful information on a_{ij} and $b_{ij}^{(p)}$. For simplicity, we assume dual porosity (two pore sets) that can be easily extended to $n > 2$ considerations.

4.1 | Drained test, long-time limit

In this test type, pressure throughout the pores is in equilibrium and constant. In other words, $p_f^{(1)} = p_f^{(2)} = 0$. Hence, strains from Equation (4) are simplified to $\mathbf{e} = \mathbf{S}\boldsymbol{\sigma}$. In such drained conditions, the elastic compliances ($S_{ijk\ell}$) can be determined. In the case of isotropy, we get $a_{11} = 1/K$, where K is the drained bulk modulus.

4.2 | Undrained test, long-time limit

This scenario provides us with the first constraint of the theory, assuming that weak connections exist between sets. If a rock sample has a closed system—so that the total fluid content change, ζ_{tot}, is zero—we get,

$$\zeta_{tot} := \zeta^{(1)} + \zeta^{(2)} = 0 \,,$$

and after a sufficiently long time,

$$p_f^{(1)} = p_f^{(2)} = p_f \,.$$

In this way, we obtain the following constraints

$$e_{ij} = \sum_{k=1}^{3} \sum_{\ell=1}^{3} S_{ijk\ell} \sigma_{k\ell} + \left(b_{ij}^{(1)} + b_{ij}^{(2)} \right) p_f \tag{6}$$

and

$$p_f = -\frac{1}{a_{22} + 2a_{23} + a_{33}} \sum_{k=1}^{3} \sum_{\ell=1}^{3} \left(b_{k\ell}^{(1)} + b_{k\ell}^{(2)} \right) \sigma_{k\ell} \,. \tag{7}$$

These are valid only if the sets are not isolated (pressure equilibration over time is possible). In the case of uniaxial stress, we can derive bulk Skempton coefficients from (7),

$$-\frac{p_f}{\sigma_{kl}} \bigg|_{\zeta_{tot}=0} \equiv \frac{1}{3} B_{k\ell} = \frac{b_{k\ell}^{(1)} + b_{k\ell}^{(2)}}{a_{22} + 2a_{23} + a_{33}} \,, \tag{8}$$

and obtain the undrained elastic compliances $S_{ijk\ell}^{u}$ from (6),

$$\frac{e_{ij}}{\sigma_{k\ell}} \bigg|_{\zeta_{tot}=0} \equiv S_{ijk\ell}^{u} = S_{ijk\ell} - \frac{1}{3} \left(b_{ij}^{(1)} + b_{ij}^{(2)} \right) B_{k\ell} \,. \tag{9}$$

Note that due to the pressure equilibration, the aforementioned bulk Skempton coefficients are equivalent to the Skempton coefficients of a single-porosity system.

4.3 | Fluid injection test, long-time limit

Another constraint may be derived if we perform a standard test of fluid injection, where the applied stress is constant ($\boldsymbol{\sigma} = \mathbf{0}$). We can again assume that the pore pressure equilibrates throughout the medium. This way, we may get the third (and last) long-time constraint

$$
\left.\frac{\zeta_{tot}}{p_f}\right|_{\boldsymbol{\sigma}=\mathbf{0}} \equiv S = a_{22} + 2a_{23} + a_{33} \tag{10}
$$

that describes the storage coefficient of the bulk medium equivalent to the storage of a single-porosity system. Note that upon combining (8)–(10), the undrained compliances are

$$
S^u_{ijk\ell} = S_{ijk\ell} + \Delta_{ijk\ell} := S_{ijk\ell} - \frac{1}{9} S B_{ij} B_{k\ell} \,, \tag{11}
$$

where $\Delta_{ijk\ell}$ is defined as the difference between the undrained and drained compliance tensors; hence, it accounts for the effect of fluids.

4.4 | Fluid injection test, drained first set

Consider another scenario where again, the applied stress is constant $\boldsymbol{\sigma} = \mathbf{0}$. Let the fluid be injected directly into the first set (e.g., background pore space) so that upon a longer time, it becomes drained, $p_f^{(1)} = 0$, since fluid migrated towards the second set. If sets are weakly connected, it may happen that the pressure in the second set is—on average—still changing due to the fluid outflow. On the other hand, the change of fluid content is almost null at the connection points between sets. Hence, we consider a period when pore pressures in a medium are not equilibrated yet, $p_f^{(2)} \neq 0$.

Another experiment can lead to $\boldsymbol{\sigma} = \mathbf{0}$, $p_f^{(1)} = 0$, and $p_f^{(2)} \neq 0$ if the fluid was injected in the second set, and in a short period, it did not have enough time to migrate towards another set. This way, the first set could remain dry (or drained).

In the case of either experiment, we get

$$
e_{ij} = b_{ij}^{(2)} p_f^{(2)} \,,
$$

$$
\zeta^{(1)} = a_{23} p_f^{(2)} \,,
$$

$$
\zeta^{(2)} = a_{33} p_f^{(2)} \,.
$$

Thus, we can define

$$
\left.\frac{e_{ij}}{p_f^{(2)}}\right|_{\boldsymbol{\sigma}=\mathbf{0},\, p_f^{(1)}=0} := b_{ij}^{(2)} \,, \tag{12}
$$

$$
\left.\frac{\zeta^{(1)}}{p_f^{(2)}}\right|_{\boldsymbol{\sigma}=\mathbf{0},\, p_f^{(1)}=0} \equiv S^{(1,2)} := a_{23} \,, \tag{13}
$$

$$
\left.\frac{\zeta^{(2)}}{p_f^{(2)}}\right|_{\boldsymbol{\sigma}=\mathbf{0},\, p_f^{(1)}=0} \equiv S^{(2)} := a_{33} \,, \tag{14}
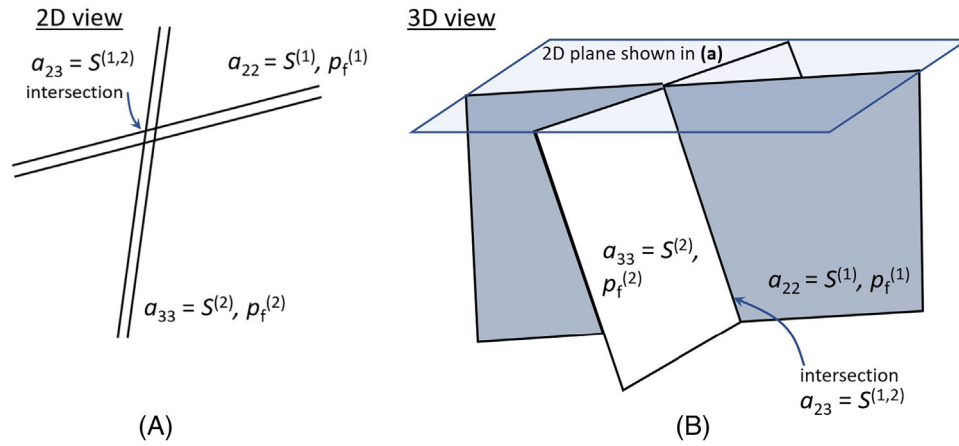$$

FIGURE 4 Schematic illustration showing different pore sets and how the terms in Equations (13)–(14), and (16) relate to physical objects. The coefficient a_{23} is the cross-term describing the storage coefficient of the intersections of set 1 and set 2. A mapping of this term to the example of two intersecting fracture sets is shown in 2D (A) and 3D (B).

where $b_{ij}^{(2)}$ is viewed as a poroelastic expansion due to fluids in the second set, scalar $S^{(1,2)}$ is the storage coefficients of weak connections between both sets, and $S^{(2)}$ is the storage coefficients of the second set. If sets are isolated, $a_{23} = 0$. It makes sense that isolated sets lead to $S^{(1,2)} = 0$ since there are no connections where the fluid could be stored. In Figure 4, we illustrate the physical meaning of a_{ij} by considering sets 1 and 2 as two independent fractures with storages $S^{(1)} = a_{22}$, and $S^{(2)} = a_{33}$, respectively. Their connection would correspond to their intersection line, which holds its own storage $S^{(1,2)} = a_{23}$.

4.5 | Fluid injection test, drained second set

If the set numbers are interchanged, then an analogous fluid injection experiments can be performed, where $\sigma = 0$, $p_f^{(2)} = 0$, and $p_f^{(1)} \neq 0$. We obtain,

$$e_{ij} = b_{ij}^{(1)} p_f^{(1)} ,$$

$$\zeta^{(1)} = a_{22} p_f^{(1)} ,$$

$$\zeta^{(2)} = a_{23} p_f^{(1)}$$

and define

$$\left. \frac{e_{ij}}{p_f^{(1)}} \right|_{\sigma=0,\, p_f^{(2)}=0} := b_{ij}^{(1)} , \tag{15}$$

$$\left. \frac{\zeta^{(1)}}{p_f^{(1)}} \right|_{\sigma=0,\, p_f^{(2)}=0} \equiv S^{(1)} := a_{22} , \tag{16}$$

$$\left. \frac{\zeta^{(2)}}{p_f^{(1)}} \right|_{\sigma=0,\, p_f^{(2)}=0} \equiv S^{(2,1)} := a_{23} = S^{(1,2)} , \tag{17}$$

where $b_{ij}^{(1)}$ is the poroelastic expansion due to fluids in the first set, and $S^{(1)}$ is the storage coefficient of this set (see Figure 4).

4.6 | Undrained first set, drained second set

Consider an abrupt change of stress imposed on a jacketed sample. Assume that fluid outflows from the second set due to the insertion of a tube ($p_f^{(2)} = 0$), whereas the first set remains approximately closed ($\zeta^{(1)} = 0$). Such a short-time experiment can work only if there is very little or no flow between sets—that is also required by the theory extension. We obtain,

$$e_{ij} = \sum_{k=1}^{3} \sum_{\ell=1}^{3} S_{ijk\ell} \sigma_{k\ell} + b_{ij}^{(1)} p_f^{(1)},$$

$$0 = \sum_{i=1}^{3} \sum_{j=1}^{3} b_{ij}^{(1)} \sigma_{ij} + a_{22} p_f^{(1)},$$

$$\zeta^{(2)} = \sum_{i=1}^{3} \sum_{j=1}^{3} b_{ij}^{(2)} \sigma_{ij} + a_{23} p_f^{(1)}.$$

Assuming the uniaxial stress, we can define

$$-\frac{p_f^{(1)}}{\sigma_{ij}}\bigg|_{\zeta^{(1)}=0,\, p_f^{(2)}=0} \equiv \frac{1}{3} B_{ij}^{(1)} := \frac{b_{ij}^{(1)}}{a_{22}}, \qquad \frac{e_{ij}}{\sigma_{k\ell}}\bigg|_{\zeta^{(1)}=0,\, p_f^{(2)}=0} \equiv S_{ijk\ell}^{u\,(1)} := S_{ijk\ell} - \frac{1}{3} b_{ij}^{(1)} B_{k\ell}^{(1)}, \tag{18}$$

where $B_{ij}^{(1)}$ is the Skempton-like tensor of the first set and $S_{ijk\ell}^{u\,(1)}$ is the undrained compliance tensor of the first set. Now the meaning of $b_{ij}^{(1)}$ becomes more tangible since knowing the definition of a_{22} we can write

$$b_{ij}^{(1)} := \frac{1}{3} S^{(1)} B_{ij}^{(1)}. \tag{19}$$

Having (19), we notice that definition of $S_{ijk\ell}^{u\,(1)}$ is analogous to the meaning of $S_{ijk\ell}^{u}$ from (11), namely,

$$S_{ijk\ell}^{u\,(1)} = S_{ijk\ell} + \Delta_{ijk\ell}^{(1)} := S_{ijk\ell} - \frac{1}{9} S^{(1)} B_{ij}^{(1)} B_{k\ell}^{(1)},$$

where $\Delta_{ijk\ell}^{(1)}$ accounts for the effect of fluid caused by the first set.

4.7 | Undrained second set, drained first set

In the analogous test, the order of sets is switched. This way, $p_f^{(1)} = 0$ and $\zeta^{(2)} = 0$. In the case of uniaxial stress, we get

$$-\frac{p_f^{(2)}}{\sigma_{ij}}\bigg|_{\zeta^{(2)}=0,\, p_f^{(1)}=0} \equiv \frac{1}{3} B_{ij}^{(2)} := \frac{b_{ij}^{(2)}}{a_{33}}, \qquad \frac{e_{ij}}{\sigma_{k\ell}}\bigg|_{\zeta^{(1)}=0,\, p_f^{(2)}=0} \equiv S_{ijk\ell}^{u\,(1)} := S_{ijk\ell} - \frac{1}{3} b_{ij}^{(1)} B_{k\ell}^{(1)} \tag{20}$$

and

$$b_{ij}^{(2)} := \frac{1}{3} S^{(2)} B_{ij}^{(2)}, \tag{21}$$

$$S_{ijk\ell}^{u\,(2)} = S_{ijk\ell} + \Delta_{ijk\ell}^{(2)} := S_{ijk\ell} - \frac{1}{9} S^{(2)} B_{ij}^{(2)} B_{k\ell}^{(2)}.$$

TABLE 1 Number of boundary test types for n-set extension.

Pressure equilibration	Required test types
Possible (weak connections)	$1^* + \dot{2} + \hat{n}$
Impossible (all sets isolated)	$1^* + \hat{n}$

Note: The required number determines drained compliances (asterix), constraints coming from long-time pressure equilibration (dot), and coefficients a_{ij} and $b_{ij}^{(p)}$ (hat). poroelastic coefficients can be determined directly (fluid-injection tests) or indirectly ("drained-undrained" tests).

4.8 | Summary of conditions

Let us discuss each scenario (test type), where different boundary conditions were assumed. First, we point out three test types that require a long-time limit. Naturally, a drained, long-time test type is indispensable to determine compliances, $S_{ijk\ell}$. Further, two scenarios from Sections 4.2 and 4.3 are important to establish the constraints (6), (7), and (10). They are necessary only if sets are not perfectly isolated. In other words, in the case of isolated sets, we need one test type only (drained, long-time). Note that the amount of required test types is not affected by the number of sets embedded in the solid matrix. Boundary conditions from Sections 4.1–4.3 can be straightforwardly translated into $n > 2$ considerations without the necessity of introducing new scenarios.

Further, let us indicate those scenarios that determine a_{ij} and $b_{ij}^{(p)}$, and where a long-time limit is not required. In the case of dual porosity, to determine a_{ij} and $b_{ij}^{(p)}$, we need only two types of tests. A reader can choose to either perform the fluid injection tests presented in Sections 4.4–4.5 or perform the "drained-undrained" tests from Sections 4.6–4.7. In the first possibility, a_{ij} (defined as storages) and $b_{ij}^{(p)}$ (defined as poroelastic expansions) are directly measured (12)–(17). In the second possibility, a combination of measured Skempton-like tensors and undrained compliances lead to indirect determination of a_{ij} and $b_{ij}^{(p)}$. Specifically, Equation (18) gives a_{22} and $b_{ij}^{(1)}$, Equation (20) provides a_{33} and $b_{ij}^{(2)}$, and additional Equation (10) from fluid-injection long-time test gives remaining a_{23}. In the case of multiple pore sets, we require additional scenarios to determine all $\{a_{ij}^{(1)}, b_{ij}^{(1)}\}, ..., \{a_{ij}^{(n)}, b_{ij}^{(n)}\}$. In the fluid injection tests, all sets except one must be drained (n combinations in total). The alternative tests that determine Skempton-like tensors and undrained compliances also require the sets to be drained except for one that needs to be undrained (again n combinations in total). The exact amount of test types can be easily deduced and is listed in Table 1.

We understand that these kinds of experiments will be difficult to achieve in practice, especially the separate control of drained and undrained behaviour in distinct sets of pores or cracks. However, we make the following points in support of our intention to help guide the design of future experiments to test the predictions of multi-porous extensions to poroelasticity theory. Firstly, we note that until now it has been almost impossible to measure undrained pore pressure changes with any accuracy or consistency within an experimental rock sample, but the recent development and validation of miniaturized (mm-scale) pore fluid pressure transducers now allows multiple, rapid (quasi-instantaneous), and localized changes in pore fluid pressure to be measured continuously during rock deformation experiments and thus allow in situ undrained poroelastic coefficients to be determined accurately for the first time.[53,63–65] Secondly, we have recently designed and 3-D printed synthetic rock-like samples with carefully designed arrays of pores and cracks of known geometry that, when filled with fluid, should exhibit a multi-porous poroelastic response.[66] Taken together, these new technical developments illuminate a clear path forwards to begin testing theoretical advances in multi-porous extensions to poroelasticity.

5 | ALTERNATIVE FORMULATIONS OF STRAIN-STRESS RELATIONS

It might be beneficial to reformulate strain-stress relations by describing a_{ij} and $b_{ij}^{(p)}$ in terms of storages and Skempton-like coefficients, as shown in (13)-(14), (16), (19), and (21). We can rewrite Equation (4) in the tensorial notation as,

$$e_{ij} = \sum_{k=1}^{3} \sum_{\ell=1}^{3} S_{ijk\ell}\sigma_{k\ell} + \frac{1}{3}S^{(1)}B_{ij}^{(1)}p_f^{(1)} + \frac{1}{3}S^{(2)}B_{ij}^{(2)}p_f^{(2)},$$

$$\zeta^{(1)} = \frac{1}{3}S^{(1)}\sum_{k=1}^{3}\sum_{\ell=1}^{3}B_{k\ell}^{(1)}\sigma_{k\ell} + S^{(1)}p_f^{(1)} + S^{(1,2)}p_f^{(2)},$$

$$\zeta^{(2)} = \frac{1}{3}S^{(2)}\sum_{k=1}^{3}\sum_{\ell=1}^{3}B_{k\ell}^{(2)}\sigma_{k\ell} + S^{(1,2)}p_f^{(1)} + S^{(2)}p_f^{(2)},$$

where in the idealized case of perfectly isolated sets, $S^{(1,2)} = 0$. Having storage and Skempton-like coefficients that describe each set, we rewrite multi-porous Equation (5) as

$$e_{ij} = \sum_{k=1}^{3}\sum_{\ell=1}^{3}S_{ijk\ell}\sigma_{k\ell} + \sum_{p=1}^{n}\frac{1}{3}S^{(p)}B_{ij}^{(p)}p_f^{(p)}, \tag{22}$$

$$\zeta^{(p)} = \frac{1}{3}S^{(p)}\sum_{k=1}^{3}\sum_{\ell=1}^{3}B_{k\ell}^{(p)}\sigma_{k\ell} + S^{(p)}p_f^{(p)} + \sum_{q=1}^{n}S^{(p,q)}p_f^{(q)}, \tag{23}$$

where $q \in \mathbb{N}$, $1 \leq q \leq n$, and $q \neq p$. If certain set p is isolated from q, then $S^{(p,q)} = 0$. The equations for all isolated sets are given and discussed explicitly in our parallel paper.[33]

So far, we have presented two versions of strain-stress relations for a multiple-porosity system. Equations (5) used coefficients $a_{ij}^{(p)}$ and $b_{ij}^{(p)}$, whereas Equations (22)-(23) utilized more tangible Skempton-like and storage coefficients. Below, we introduce new parameters that facilitate the alternative description of equations relating strains and stresses useful for further, time-dependent analysis. After algebraic manipulations on Equations (22)–(23), we obtain mixed strain-stress formulations,

$$\sigma_{ij} = \sum_{k=1}^{3}\sum_{\ell=1}^{3}C_{ijk\ell}e_{k\ell} - \sum_{p=1}^{n}\alpha_{ij}^{(p)}p_f^{(p)}, \tag{24}$$

$$\zeta^{(p)} = \sum_{k=1}^{3}\sum_{\ell=1}^{3}\alpha_{k\ell}^{(p)}e_{k\ell} + \frac{1}{M^{(p)}}p_f^{(p)} + \sum_{q=1}^{n}\frac{1}{M^{(p,q)}}p_f^{(q)}, \tag{25}$$

where again $q \in \mathbb{N}$, $1 \leq q \leq n$, $q \neq p$, and $C_{ijk\ell}$ denotes elasticity tensor. Further,

$$\alpha_{ij}^{(p)} := \frac{1}{3}S^{(p)}\sum_{k=1}^{3}\sum_{\ell=1}^{3}C_{ijk\ell}B_{k\ell}^{(p)} \tag{26}$$

is the Biot-like tensor for each set of pores and

$$\frac{1}{M^{(p)}} := S^{(p)} - \sum_{i=1}^{3}\sum_{j=1}^{3}\sum_{k=1}^{3}\sum_{\ell=1}^{3}S_{ijk\ell}\alpha_{ij}^{(p)}\alpha_{k\ell}^{(p)}, \tag{27}$$

$$\frac{1}{M^{(p,q)}} := S^{(p,q)} - \sum_{i=1}^{3}\sum_{j=1}^{3}\sum_{k=1}^{3}\sum_{\ell=1}^{3}S_{ijk\ell}\alpha_{ij}^{(p)}\alpha_{k\ell}^{(q)}$$

describe fluid storage under no frame deformation. To grasp the physical meaning of the above-mentioned coefficients, let us think of fluid injection tests analogous to the ones from Section 4.4–4.5, where $\mathbf{e} = \mathbf{0}$ instead of $\boldsymbol{\sigma} = \mathbf{0}$ is required. Then, we obtain

$$\left.\frac{\sigma_{ij}}{p_f^{(2)}}\right|_{\mathbf{e}=\mathbf{0},\,p_f^{(1)}=0} \equiv -\alpha_{ij}^{(2)},$$

$$\left.\frac{\zeta^{(1)}}{p_f^{(2)}}\right|_{\mathbf{e}=\mathbf{0},\,p_f^{(1)}=0} \equiv \frac{1}{M^{(1,2)}},$$

$$\left.\frac{\zeta^{(2)}}{p_f^{(2)}}\right|_{\mathbf{e}=\mathbf{0},\, p_f^{(1)}=0} \equiv \frac{1}{M^{(2)}}$$

and

$$\left.\frac{\sigma_{ij}}{p_f^{(1)}}\right|_{\mathbf{e}=\mathbf{0},\, p_f^{(2)}=0} \equiv -\alpha_{ij}^{(2)},$$

$$\left.\frac{\zeta^{(1)}}{p_f^{(1)}}\right|_{\mathbf{e}=\mathbf{0},\, p_f^{(2)}=0} \equiv \frac{1}{M^{(1)}},$$

$$\left.\frac{\zeta^{(2)}}{p_f^{(1)}}\right|_{\mathbf{e}=\mathbf{0},\, p_f^{(2)}=0} \equiv \frac{1}{M^{(2,1)}} = \frac{1}{M^{(1,2)}},$$

respectively. Note that definitions (26) and (27) are analogous to the Cheng[67] definitions for single porosity (his equations (20) and (22)). The mixed formulation will be explicitly used in the consolidation equations in the next section. Also, one can try to introduce stress-strain relations by switching $\zeta^{(p)}$ with $p_f^{(p)}$ and reformulating poroelastic coefficients.[27] However, in contrast to the original Biot theory, such a formulation may become complicated due to the existence of multiple pore pressures. In a simpler case of isolated sets, we obtain

$$\sigma_{ij} = \sum_{i=1}^{3}\sum_{j=1}^{3} C_{ijk\ell}^{u} e_{k\ell} - \sum_{p=1}^{n} M^{(p)}\alpha_{ij}^{(p)}\zeta^{(p)}, \tag{28}$$

$$p_f^{(p)} = -M^{(p)}\sum_{k=1}^{3}\sum_{\ell=1}^{3} \alpha_{k\ell}^{(p)} e_{k\ell} + M^{(p)}\zeta^{(p)}, \tag{29}$$

where the undrained elasticity parameters

$$C_{ijk\ell}^{u} := C_{ijk\ell} + \sum_{p=1}^{n} M^{(p)}\alpha_{ij}^{(p)}\alpha_{k\ell}^{(p)}.$$

Stress-strain relations for a more complicated case of weakly-connected sets are given in the Appendix.

6 | GOVERNING EQUATIONS OF CONSOLIDATION

Herein, we study the governing equations that describe the transient phenomenon of three-dimensional consolidations. These are differential equations governing the distributions of stress and fluid content change and settlement as a function of time in a medium under given loads. If a fluid content is increased due to an increase in the volume of pores, the governing equations describe the opposite process of swelling instead of consolidation. For convenience, we derive the case of dual porosity. Nevertheless, at the end of the section, the multi-porous generalization is additionally presented. Note that, as discussed by Biot[68] for single-porosity case and by Borja and Koliji[69] for dual-porosity, a similar procedure can be followed to establish general solutions using laws of thermodynamics. This way, the energy-conjugate variables can be identified and the expression for the effective stress that is energy-conjugate to the rate of deformation of the solid matrix can be derived.[29]

To obtain the governing equations, first, changes in externally applied stresses must satisfy the equilibrium conditions; namely,

$$\sum_{j=1}^{3} \frac{\partial \sigma_{ij}}{\partial x_j} = 0 \,. \tag{30}$$

We assume that body forces can be neglected. Then, we insert (24) into (30) and rewrite strains in terms of displacements (1). We obtain three governing equations

$$\sum_{j=1}^{3} \left[\sum_{k=1}^{3} \sum_{\ell=1}^{3} \frac{1}{2} C_{ijk\ell} \left(\frac{\partial u_k}{\partial x_j \partial x_\ell} + \frac{\partial u_\ell}{\partial x_j \partial x_k} \right) - \alpha_{ij}^{(1)} \frac{\partial p_f^{(1)}}{\partial x_j} - \alpha_{ij}^{(2)} \frac{\partial p_f^{(2)}}{\partial x_j} \right] = 0 \,. \tag{31}$$

To obtain the rest of the governing equations, let us define the flux of the fluid through pore set p as

$$q_i^{(p)} := \phi^{(p)} \left(\frac{\partial U_i^{(p)}}{\partial t} - \frac{\partial u_i}{\partial t} \right). \tag{32}$$

Having defined the fluid content changes (2) and the fluid flux (32), we can formulate the equations of fluid continuity. Assuming that the fluid is incompressible and that a certain amount diffuses internally,

$$\sum_{i=1}^{3} \frac{\partial q_i^{(1)}}{\partial x_i} + \frac{\partial \zeta^{(1)}}{\partial t} + \frac{\partial \zeta^{(1,2)}}{\partial t} = 0 \,, \tag{33}$$

$$\sum_{i=1}^{3} \frac{\partial q_i^{(2)}}{\partial x_i} + \frac{\partial \zeta^{(2)}}{\partial t} + \frac{\partial \zeta^{(2,1)}}{\partial t} = 0 \,, \tag{34}$$

where the interset fluid flow

$$\frac{\partial \zeta^{(p,q)}}{\partial t} := \Gamma^{(p,q)} \left(p_f^{(p)} - p_f^{(q)} \right)$$

is assumed to be proportional to the difference in pore pressures. Equations (33)–(34) state that the external change in the amount of fluid in a pore set at any instant is balanced by the fluid flowing into the set whilst a certain amount of fluid is diffused inside the medium. It is required that $\partial \zeta^{(1,2)} / \partial t = -\partial \zeta^{(2,1)} / \partial t$ since the internal diffusion between the sets must be equal; fluid volume is assumed to be conserved and not compressed. Note that in the case of $n > 2$ sets, there is more than a single leakage constant Γ. For instance, if $n = 4$, we get six possibilities, namely, $\Gamma^{(1,2)}, \Gamma^{(1,3)}, \Gamma^{(1,4)}, \Gamma^{(2,3)}, \Gamma^{(2,4)}$, and $\Gamma^{(3,4)}$. In total, there are $\sum_{p=1}^{n} (n - p)$ leakage constants.

Now, let us invoke a crucial constitutive relation. Darcy's law for dual porosity can be written as

$$q_i^{(1)} = -\sum_{j=1}^{3} \frac{k_{ij}^{(1)}}{\mu} \frac{\partial p_f^{(1)}}{\partial x_j} - \sum_{j=1}^{3} \frac{k_{ij}^{(1,2)}}{\mu} \frac{\partial p_f^{(2)}}{\partial x_j} \,, \tag{35}$$

$$q_i^{(2)} = -\sum_{j=1}^{3} \frac{k_{ij}^{(2)}}{\mu} \frac{\partial p_f^{(2)}}{\partial x_j} - \sum_{j=1}^{3} \frac{k_{ij}^{(2,1)}}{\mu} \frac{\partial p_f^{(1)}}{\partial x_j} \,, \tag{36}$$

where μ denotes viscosity. Fluid is assumed to be of the same type throughout the medium. Note that (35)–(36) are the anisotropic extensions of Aifantis[12] expressions. We can combine the aforementioned Darcy's law (35)–(36) with the continuity Equations (33)–(34) and fluid content changes from strain-stress relations (25). This way, we obtain the remaining set of governing equations, namely,

$$\sum_{i=1}^{3}\sum_{j=1}^{3}\left(\frac{k_{ij}^{(1)}}{\mu}\frac{\partial^2 p_f^{(1)}}{\partial x_i \partial x_j} + \frac{k_{ij}^{(1,2)}}{\mu}\frac{\partial^2 p_f^{(2)}}{\partial x_i \partial x_j}\right) + \Gamma\left(p_f^{(2)} - p_f^{(1)}\right) =$$

$$\frac{1}{2}\sum_{i=1}^{3}\sum_{j=1}^{3}\alpha_{ij}^{(1)}\frac{\partial}{\partial t}\left(\frac{\partial u_i}{\partial x_j} + \frac{\partial u_j}{\partial x_i}\right) + \frac{1}{M^{(1)}}\frac{\partial p_f^{(1)}}{\partial t} + \frac{1}{M^{(1,2)}}\frac{\partial p_f^{(2)}}{\partial t}\,,$$

(37)

$$\sum_{i=1}^{3}\sum_{j=1}^{3}\left(\frac{k_{ij}^{(2)}}{\mu}\frac{\partial^2 p_f^{(2)}}{\partial x_i \partial x_j} + \frac{k_{ij}^{(2,1)}}{\mu}\frac{\partial^2 p_f^{(1)}}{\partial x_i \partial x_j}\right) + \Gamma\left(p_f^{(1)} - p_f^{(2)}\right)$$

$$= \frac{1}{2}\sum_{i=1}^{3}\sum_{j=1}^{3}\alpha_{ij}^{(2)}\frac{\partial}{\partial t}\left(\frac{\partial u_i}{\partial x_j} + \frac{\partial u_j}{\partial x_i}\right) + \frac{1}{M^{(2)}}\frac{\partial p_f^{(2)}}{\partial t} + \frac{1}{M^{(1,2)}}\frac{\partial p_f^{(1)}}{\partial t}\,.$$

(38)

Three differential Equations (31) for stress distribution and two diffusion Equations (37)–(38) for the fluid flow, determine five unknowns, u_i, $p_f^{(1)}$, and $p_f^{(2)}$. For n pore-sets, the governing equations are rewritten as

$$\sum_{j=1}^{3}\left[\sum_{k=1}^{3}\sum_{\ell=1}^{3}\frac{1}{2}C_{ijk\ell}\left(\frac{\partial u_k}{\partial x_j \partial x_\ell} + \frac{\partial u_\ell}{\partial x_j \partial x_k}\right) - \sum_{p=1}^{n}\alpha_{ij}^{(p)}\frac{\partial p_f^{(p)}}{\partial x_j}\right] = 0\,,$$

(39)

$$\sum_{i=1}^{3}\sum_{j=1}^{3}\left(\frac{k_{ij}^{(p)}}{\mu}\frac{\partial^2 p_f^{(p)}}{\partial x_i \partial x_j} + \sum_{q=1}^{n}\frac{k_{ij}^{(p,q)}}{\mu}\frac{\partial^2 p_f^{(q)}}{\partial x_i \partial x_j}\right) - \sum_{q=1}^{n}\Gamma^{(p,q)}\left(p_f^{(p)} - p_f^{(q)}\right) =$$

$$\frac{1}{2}\sum_{i=1}^{3}\sum_{j=1}^{3}\alpha_{ij}^{(p)}\frac{\partial}{\partial t}\left(\frac{\partial u_i}{\partial x_j} + \frac{\partial u_j}{\partial x_i}\right) + \frac{1}{M^{(p)}}\frac{\partial p_f^{(p)}}{\partial t} + \sum_{q=1}^{n}\frac{1}{M^{(p,q)}}\frac{\partial p_f^{(q)}}{\partial t}\,.$$

(40)

There are $n + 3$ equations that determine $n + 3$ unknowns, u_i, $p_f^{(1)}, \ldots, p_f^{(n)}$.

7 | NUMERICAL EXAMPLES

Let us consider numerical examples to demonstrate the usage of consolidation equations. In our simulations, we go beyond the typical setting of single or dual porosity assumed in the past. Herein, we consider triple porosity, where a medium contains micropores, macropores, and fractures. Also, we allow different mechanical and diffusion properties of a pore set. The solutions of the partial differential equations were obtained using the integral finite difference method to solve the fluid flow problem (through porous media) and the virtual element method (VEM) to solve the solid mechanics problem. These methods were implemented inside the Matlab Reservoir Simulation Toolbox, MRST.[70] Within MRST, we generalized a dual-porosity module provided by Ashworth and Doster[71] to fit our multi-porous extension. Although our examples have illustration purposes only, they are selected in such a way to mimic a probable geological scenario. Note that our simulations differ from Mehrabian and Abousleiman[72] since we do not explicitly assume hierarchical type of porosity, we do not assume harmonic average of porosity systems and we check the influence of different values of poroelastic and permeability parameters on fluid pressure changes over time.

7.1 | Model conditions and parameters

We choose the following geometrical setting and stress-strain boundary conditions (Figure 5). The considered medium is 2 m $\times$ 2 m with a regular 20 $\times$ 20 mesh. Changes in fluid pressures are induced by external compressional stress of 1 MPa imposed on the top side. Displacements are vertical only. The fluid is allowed to flow through the top boundary only. Medium is considered to be undrained at a time $t = 0$. At the beginning of the consolidation, the material is intact and has the properties discussed in the paragraph below and schematically presented in Figure 5.
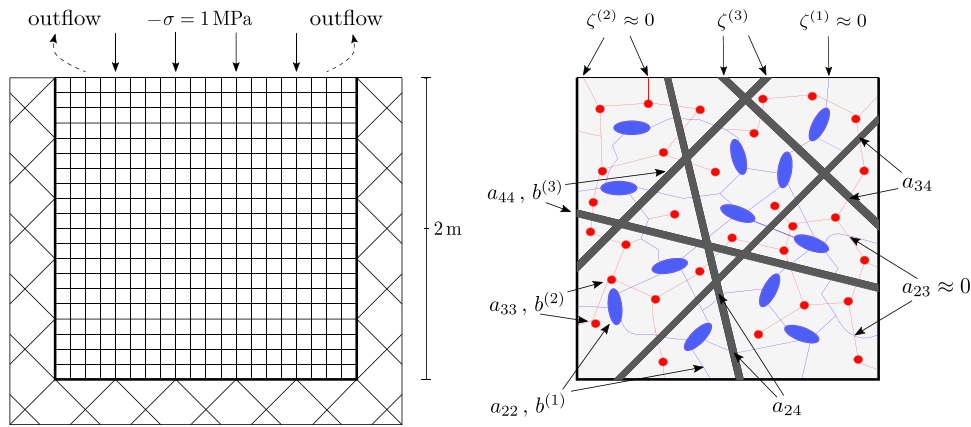
FIGURE 5 On the left: sketch of a geometrical setting, stress, and flow conditions. On the right: sketch of a triple-porosity scenario with a mapping of selected poroelastic coefficients. Connected macropores (set 1) are in blue, micropores (set 2) in red, and fractures (set 3) in black. Macro- and micro-porosity are treated as isolated from each other, whereas the other sets are weakly connected. Outflow coming from the background sets (macro- and micro-porosity) is neglected.

This triple-porosity case can be typical for, for example, reservoir rocks. Although there is experimental evidence of multiple-porosity behaviour, the exact measurement of poroelastic coefficients in geomaterials remains challenging. To the best of our knowledge, the storages and Biot-like parameters extracted in the laboratory are available for the simplified isotropic dual porosity case only.[22] Therefore, similarly to other researchers, we must choose certain input values subjectively.[73] Our choices are based on the values proposed by Berryman and Pride[23] for Weber sandstone.

For the purposes of a simple calculation of the effective elasticity that is used in this study, we divide the material into three porous constituents and define,

$$v^{(c)} := \frac{V^{(c)}}{V},$$

where (c) stands for the constituent that contains one pore set (p) so that $V^{(c)} > V^{(p)}$. Remembering definition $\phi^{(p)} := V^{(p)}/V$, we obtain the following two relations

$$v^{(c)} > \phi^{(p)}$$

$$v^{(1)} + v^{(2)} + v^{(3)} = 1$$

that must hold. Constituent 1 contains a set of macropores, constituent 2 contains the set of micropores, whereas the remaining constituent contains fractures. Material and fluid characteristics can be found in Table 2. The majority of parameters corresponding to macropores and fractures are taken from Berryman and Pride.[23] The values of other coefficients—including all parameters for microporosity—are chosen by us; they are bold in Table 2.

Let us discuss the volume fractions and stiffnesses chosen. We assumed that the original volume occupied by unfractured porous background given by Berryman and Pride[23] is equally divided between constituents with macro and micropores, $v^{(1)} = v^{(2)}$, where the macroporosity itself (set 1) occupies almost twice the space of the microporosity (set 2), $\phi^{(1)} \approx 2\phi^{(2)}$. In general, Young's modulus diminishes with a higher concentration of pores.[74] Due to a smaller void space in set 2, we choose $E_s > E^{(2)} > E^{(1)}$, where E_s is Young's modulus of the solid phase, $E^{(2)}$ is the drained Young's modulus of the constituent with microporosity, and $E^{(1)}$ denotes drained Young's modulus of the constituent with macroporosity. The fractured constituent consists of a volume given by Berryman and Pride,[23] where fractures occupy most of the phase that results in a very low Young's modulus, $E^{(3)}$. According to Lutz and Zimmerman,[75] Poisson's ratio changes insignificantly when pores are spherical, and ν_s is close to 0.2. On the other hand, if cracks are considered, Poisson's ratio should diminish. Therefore, we assumed that $\nu_s = \nu^{(1)} = \nu^{(2)} > \nu^{(3)}$. To obtain the effective elasticity needed in the consolidation equations, we calculate effective Young's modulus E and effective Poisson's ratio ν by employing a Reuss average lower bound, namely,

TABLE 2 Parameters for isotropic triple-porosity simulations.

Stiffnesses			Poroel. coeff.			Fluid descr.			Volume frac.	
$E^{(1)}$	36	GPa	a_{22}	0.0993	GPa^{-1}	$k^{(1)}$	**0**	mD	$v^{(1)}$	**0.5** $\times$ 0.9905
$E^{(2)}$	**50**	GPa	a_{33}	$\boldsymbol{x\,a_{22}}$	GPa^{-1}	$k^{(2)}$	**0**	mD	$v^{(2)}$	**0.49525**
$E^{(3)}$	0.15	GPa	a_{44}	0.145	GPa^{-1}	$k^{(3)}$	z	mD	$v^{(3)}$	0.0095
$\nu^{(1)}$	0.15		$b^{(1)}$	0.0253	GPa^{-1}	$k^{(1,2)}$	**0**	mD	$\phi^{(1)}$	0.095
$\nu^{(2)}$	**0.15**		$b^{(2)}$	$\boldsymbol{y\,b^{(1)}}$	GPa^{-1}	$k^{(1,3)}$	$1/z$	mD	$\phi^{(2)}$	**0.05**
$\nu^{(3)}$	**0.12**		$b^{(3)}$	0.049	GPa^{-1}	$k^{(2,3)}$	$1/z$	mD	$\phi^{(3)}$	**0.009**
K_s	37	GPa	a_{23}	0	TPa^{-1}	$\Gamma^{(1,2)}$	**0**	$\frac{1}{\text{GPa}\times\text{s}}$		
E_s	**62.9**	GPa	a_{24}	**0.5**$\times$2.7	TPa^{-1}	$\Gamma^{(1,3)}$	$1/z$	$\frac{1}{\text{GPa}\times\text{s}}$		
ν_s	**0.15**		a_{34}	1.35	TPa^{-1}	$\Gamma^{(2,3)}$	$1/z$	$\frac{1}{\text{GPa}\times\text{s}}$		
						μ	1	cP		

Note: Specific values of unknowns x, y, z correspond to different cases discussed. Bold values are chosen subjectively by the authors. Other values were provided by Berryman and Pride[23] based on laboratory measurements.

$$E = \left(v^{(1)}\frac{1}{E^{(1)}} + v^{(2)}\frac{1}{E^{(2)}} + v^{(3)}\frac{1}{E^{(3)}} \right)^{-1} \approx 11.49\,\text{GPa}\,,$$

$$\nu = \left(v^{(1)}\frac{1}{\nu^{(1)}} + v^{(2)}\frac{1}{\nu^{(2)}} + v^{(3)}\frac{1}{\nu^{(3)}} \right)^{-1} \approx 0.149\,.$$

Now, let us discuss the values of coefficients describing fluids and poroelastic properties. We chose the typical viscosity of water at $\mu = 1$ cP, and we selected permeabilities corresponding to the well-known situation of highly permeable fractures and background pore space having very low permeability. We assume that the time-dependent external diffusion of the fluid directly from the background is negligible that is reflected by $k^{(1)} = k^{(2)} = 0$. Also, fluid does not exchange between micro and macro porosities, which is reflected by the intersection storage $a_{23} = 0$, interflow permeability $k^{(1,2)} = 0$, and leakage $\Gamma^{(1,2)} = 0$. However, fluid exchange is allowed between micropores (set 1) and fractures (set 3) as well as between macropores (set 2) and fractures. Therefore, inter-pore sets permeabilities and leakages $k^{(1,3)}$, $k^{(2,3)}$, $\Gamma^{(1,3)}$ and $\Gamma^{(2,3)} > 0$. To check the influence that the relative differences in permeability and leakage between pore sets may inflict on internal and external flux, we introduced multiplier z equal to 10, 10^3, or 10^5, which relate $k^{(p,q)}$ and $\Gamma^{(p,q)}$ as indicated in Table 2. Leakage coefficients governing the internal flow are obtained as follows.

$$\Gamma^{(p,q)} = \frac{\delta \times k^{(p,q)}\,[\text{mD}]}{(L\,[\text{m}])^2 \times \mu\,[\text{cP}]} = \frac{\pi^2 k^{(p,q)} \times 9.869233 \times 10^{-16}\,[\text{m}^2]}{\mu \times 10^{-5}\,[\text{Pa} \times \text{s} \times \text{m}^2]} \approx k^{(p,q)}\left[\frac{1}{\text{GPa} \times \text{s}}\right],$$

where δ is the shape factor[14] assumed to be equal to π^2, and $L = 0.1$ m is the fracture spacing viewed as the parameter that corresponds to the fracture concentration. To check the influence of the relative difference between pore sets in poroelastic coefficients, a_{ij}, that is, storages, and $b^{(p)}$, that is, poroelastic expansion coefficients, we introduced multipliers x and y that are respectively equal to 0.8 and 0.5, 0.5 and 0.5, or 0.5 and 0.8. Based on the work of Selvadurai and Suvorov,[76] the Biot coefficient is usually lower for a lower concentration of pores that have similar shapes. Combining (19) and (26), we can express the isotropic expansion coefficient as,

$$b^{(p)} = \frac{1}{3K}\alpha^{(p)}.$$

Hence, $b^{(p)}$ is strictly related to the Biot-like coefficient; its value is expected to be lower for lower pore concentrations. This is why the chosen values of y are below 1 to relate poroelastic expansion coefficients between macro and micropores (sets 1 and 2, respectively). In the literature, the values of fluid storage are still weakly explored, but we suspect achieving lower storage for lower pore concentrations of similar shape, which is why x is also below 1. Since the shape of the inhomogeneity can greatly affect the poroelastic coefficient,[76] the interplay of x and y can mimic different pore configurations between background constituents, that is, macro and micro pore sets.
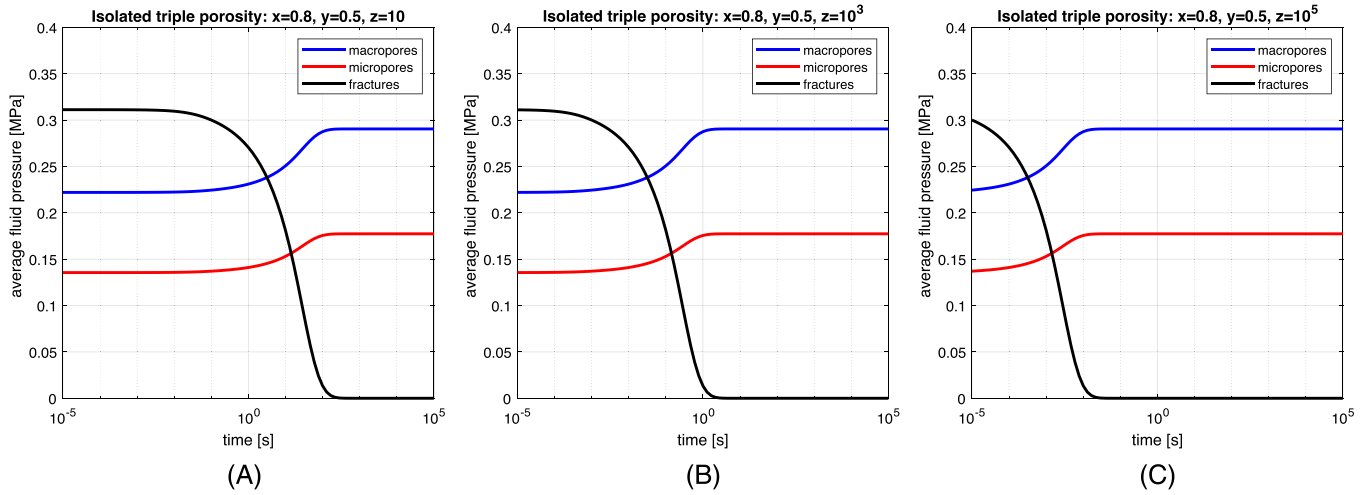
FIGURE 6 Semi-log plots of the average fluid pressure changes with time. Initially undrained triple-porosity medium with isolated sets. Microporosity and macroporosity remain undrained, whereas the fractured constituent is drained with time.

7.2 | Results

In this section, we discuss the results of the triple-porosity simulations. Specifically, we focus on the time-dependent fluid pressure changes caused by the fluid outflow and gradual drainage of the medium. Before we move to the results of the model configurations discussed previously, first, let us invoke an end member case of isolated pore sets. In other words, assume that the drainage is achieved for the fractured constituent only, whereas the background pore spaces (sets 1 and 2) remain undrained. To obtain such scenario, we set $a_{23} = a_{24} = a_{34} = 0$, $k^{(1,2)} = k^{(1,3)} = k^{(2,3)} = 0$, and $\Gamma^{(1,2)} = \Gamma^{(1,3)} = \Gamma^{(2,3)} = 0$. The rest of the parameters from Table 2 remain unchanged. The results are provided for $x = 0.8$, $y = 0.5$, and various values of z; they are illustrated in Figure 6.

We notice that the solid deformation and the drainage of fractures lead to an increase in fluid pressures of the background constituents and a decrease in fracture fluid pressure. The above phenomenon can be explained as follows. In the absence of fluid volume change within the porous background, $\zeta^{(1)} = \zeta^{(2)} = 0$, solid compression leads to the increase of a volumetric strain, e, that must be compensated by the increase of $p_f^{(1)}$ and $p_f^{(2)}$; see for example, Equation (25). Further, the increased aforementioned pressures equilibrize the decrease of $p_f^{(3)}$ caused by the fluid outflow from the fractures; see for example, Equation (24). Due to the isolation of the background sets, their pressures must increase till the drainage process is finished. Naturally, the complete drainage appears earlier for larger $k^{(3)}$. This is why $p_f^{(3)}$ approaches zero most rapidly in Figure 6C, where $k^{(3)} = 10^5$ mD, and most slowly in Figure 6A, where $k^{(3)} = 10$ mD.

Now, let us consider examples with the input values given in Table 2. In other words, we simulate the scenario of weakly-connected pore sets. Results for all combinations of x, y, and z multipliers are provided in Figure 7. Particularly, Figures 7A–C, have the same multipliers as in the previous case of isolated sets so that the isolated and connected scenarios can be compared directly.

Let us discuss the results. In Figures 7A–C, background pressures increase gradually and, upon a certain time, they start to decrease abruptly. The decrease appears earlier for larger interflow permeabilities (stronger leakage). If the interflow is small, as illustrated in Figure 7C, pressures converge with the isolated sets scenario from Figure 6C up to $t \approx 10$ s, after which macro and micropore fluid pressure abruptly decrease to zero. By contrast, we notice that a relatively small contrast in fracture and interflow permeabilities leads to pressure equilibration and single-porosity response over a short period of time, as shown in Figure 7A. An interesting bump of background pressures can be noticed in Figure 7B at $t \approx 1$ s. This can be explained as follows. Initially, some fluid volume contained in fractures drains directly from them, and background sets behave as isolated since their pressures are lower than that in fractures, which impedes internal leakage (the background is already fully saturated). Subsequently, once pressures in the background become higher, the fluid starts to diffuse towards the fractures so that the pressures equilibrize throughout the medium. However, such an equilibration process does not happen instantaneously due to the much lower interflow permeability that causes the bump. In the case of low contrast in
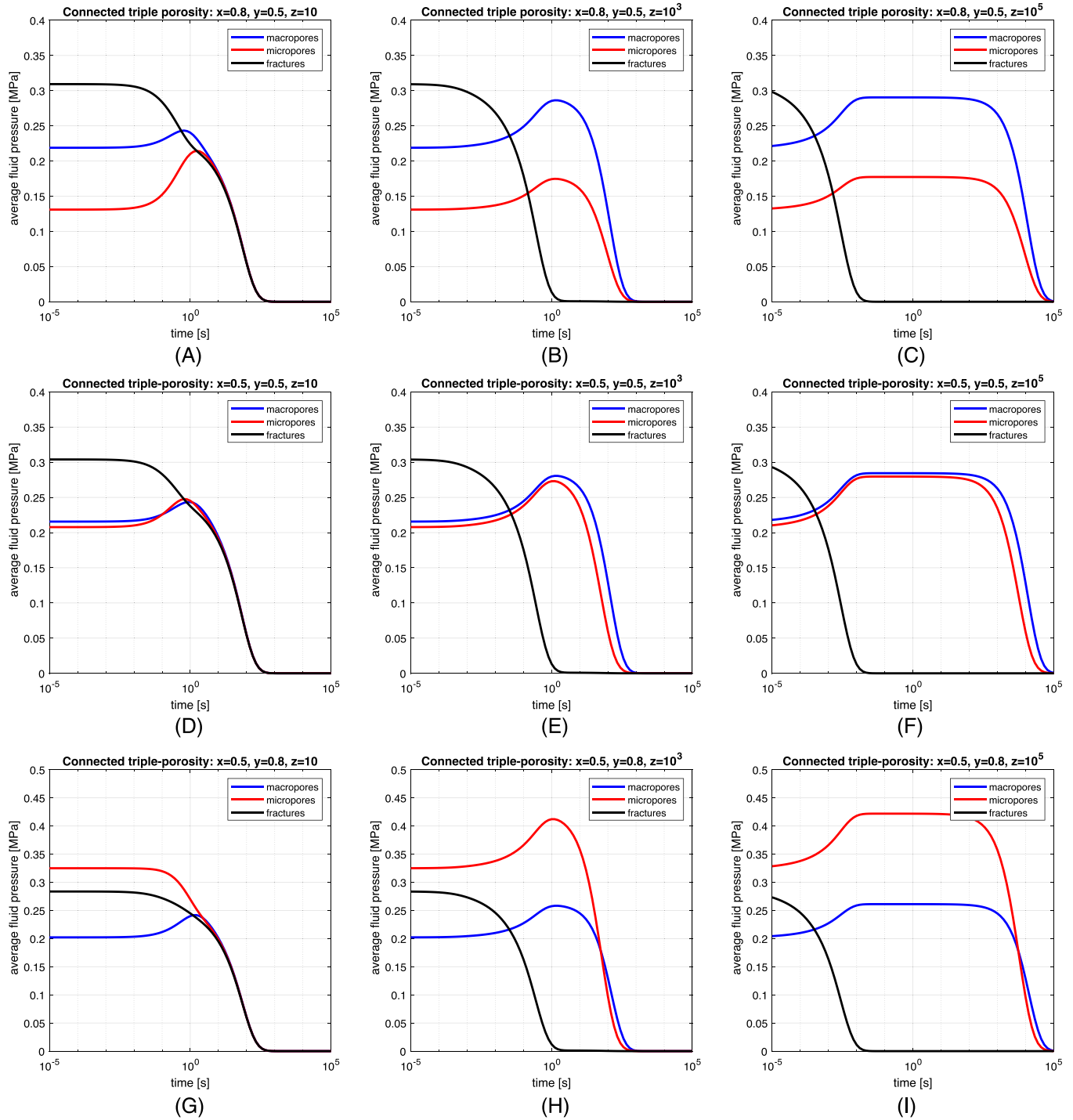
FIGURE 7 Semi-log plots of the average fluid pressure changes with time. Initially undrained triple-porosity medium with weakly-connected sets. Each set becomes drained with time.

permeabilities, the bump is hardly visible. Figures 7D–F, display the case in which multipliers $x = y = 0.5$ and therefore represent a higher contrast in poroelastic coefficients between micro and macro-pores sets. This situation exhibits similar pressure evolution to that shown in Figures 7A–C, but with very small difference between background (macro and micro pore sets) pressures. This small contrast in background pressures is representative of an almost dual-porosity response. This phenomenon of nearly dual-porosity behavior that is, micro and macro pores acting as a single set, may appear counter-intuitive considering that both storage and Biot-like coefficients are greatly diminished for the microporosity ($x = y = 0.5$) compared to the macroporosity. However, it can be explained as follows. The absence of the external outflow

from the background, $\zeta^{(1)} = \zeta^{(2)} = 0$, can be rewritten using (5) along with $a_{33} = xa_{22}$, and $b^{(2)} = yb^{(1)}$ as

$$0 = b^{(1)}\sigma + a_{22}p^{(1)} + a_{23}p^{(2)} + a_{24}p^{(3)},$$

$$0 = yb^{(1)}\sigma + a_{23}p^{(1)} + xa_{22}p^{(2)} + a_{34}p^{(3)}.$$

Knowing that intersecting storages are zero or very low, then we get

$$b^{(1)}\sigma + a_{22}p^{(1)} \approx \frac{y}{x}b^{(1)}\sigma + a_{22}p^{(2)} \tag{41}$$

therefore, if $x = y$, then $p^{(1)} \approx p^{(2)}$. In consequence, the ratio between x and y—not just their absolute values—influences substantially the relationship between micro and macro-porosity pressure evolution. The importance of poroelastic coefficients in the consolidation process is again confirmed in Figures 7G–I. These figures represent a case of relatively low storage and high Biot-like coefficients that cause high fluid pressure in microporosity.

Our simulations show the consolidation process in multi-porous media and provide certain insights on time-dependent changes in fluid pressures. We demonstrated that the pressure evolution and pore sets interplay is controlled by the relative differences in permeability and poroelastic coefficients between pore sets. By considering different combinations of pore sets permeabilities and poroelastic coefficients, we showed specific scenarios where the triple-porosity case converges to single or dual-porosity responses. In particular, a triple porosity medium will rapidly converge to a single porosity medium if the contrast between the permeability of the most permeable pore set (fractures in this example) and the inter-pore sets permeability is small (less than two orders of magnitude difference in this example) (Figures 7A,D,G). We also identified characteristic features, such as pressure "bumps" (Figures 7B,E,H) appearing in the consolidation process when the contrast between fracture and inter-pore sets permeability is sufficient to cause distinctive responses between pore sets but not large enough to cause pressure equilibration in the background for a significant amount of time before draining (Figures 7C,F,I). Our examples should not be treated as conclusive but rather encourage future investigations on other multi-porous scenarios.

8 | DISCUSSION

Our multi-porous extension provides a rigorous description of an instantaneous deformation along with time-dependent fluid flow and consolidation of a solid medium containing complex porous structures. The effects of pore sets and their anisotropic responses are not neglected. To obtain such an accurate description that accounts for meso-scopic inhomogeneities (pore-sets), many coefficients are needed (see e.g., Table 2). These may be difficult to obtain in both laboratory and field measurements. Nevertheless, recent studies[53] revealed that an accurate determination of local variations in fluid pressure, at the scale of the laboratory sample, is possible. Given rapid developments in experimental geophysics, one should optimistically look to the future applicability of the multi-porous exten-sion. Further, alternative tests to the ones from Sections 4–5 are possible. First, we can consider uniform-expansion thought experiments.[24] Second, the poroelastic coefficients can be obtained from micromechanical derivations, as pre-sented in our parallel paper.[33] In the planned future developments, we will perform the experiments proposed in Sections 4–5.

Our analysis of time-dependent deformation for multi-porous anisotropic poroelasticity reveals potentially significant mechanical consequences. For both isolated (Figure 6) and weakly-connected (Figure 7) pore sets (1 and 2), the pore fluid pressure is predicted to rise as the pore fluid drains through the fractures (set 3). In the case of weakly-connected pore sets 1 and 2 shown in Figure 7, there are distinct transient peaks in pore fluid pressure of the order of several seconds duration. This means that in a draining poroelastic material with multiple pore sets such as rock loaded in a fault zone, as the fluid drains through the high permeability fractures and the pore fluid pressure drops therein, the pore fluid pressure in weakly-connected pore sets in the rock matrix increases for short periods (seconds), thereby reducing the local effective stress $\sigma_{eff} = \sigma + \alpha^{(p)}p_f^{(p)}$. The pore fluid pressure decrease in the fractures causes a local increase in effective stress. These localized changes in effective stress will push the matrix containing the weakly connected pore sets towards mechanical failure, and the fractures away from mechanical failure.[77] Moreover, it is clear from the cases modelled in Figure 7 that the magnitude and duration of the pore fluid pressure transient in the weakly-connected pore sets

(1 and 2)—and therefore the period in which the effective stress is reduced—critically depends on their relative poroelastic properties (a_{33}, $b^{(2)}$). Further analysis of this phenomenon is beyond the scope of the present work but will be addressed in a follow-up paper.

Two main alternatives to the presented multi-porous theory extension can be used to model the mechanical behaviour of complex porous structures; homogenization and discretization.[18] The medium can be homogenized and treated as poroelastically effective[78] or discretized, where local subgrid flows are determined individually.[46] However, homogenization does not allow us to distinguish different flow characteristics. Using elastic layers as an analogy, the homogenization of thin constituents makes sense from the long-wave seismic perspective, but the intrinsic properties of layers are lost. The discretization is difficult to introduce at a field scale, where fractures are abundant,[18] and the integration of the subgrids to a continuum model presented herein can cause issues.[79] If pore sets are spatially distributed (not nested, not fractured), one can try to discretize the medium to obtain a local, single—instead of multiple—porosity case (Figure 1). Nevertheless, if extended coefficients can be either measured or estimated, we recommend using the multi-porous extension as the most accurate macro-meso-mechanical description.

It seems that there is no best choice of the number of pore sets, n. We believe that in reality, at a microscale and in a short-time period, each pore within the same pore set can be characterized by slightly or even significantly different poroelastic properties. The connections between pores in a pore set are not ideal and hence, most probably, lead to pressure, permeability, and fluid increment pore-scale variations. Thus, one can choose between macroscopic single-porosity description ($n = 1$), more accurate—but still somewhat idealized—mesoscopic dual-porosity description ($n = 2$), or even more accurate mesoscopic triple-porosity description ($n = 3$), and so on ($n \geq 4$), till fully microscopic description is reached ($n =$ total number of pores).[33] Naturally, the choice of the model is a trade-off between scale refinement and the accuracy of the estimation—if at all possible—of the parameters.

9 | SUMMARY

We have proposed the multi-porous extension of anisotropic poroelasticity—quasi-static theory originally presented by Biot.[1] Our rationale for developing the generalization of anisotropic poroelasticity was a new conceptual time-dependent model of pressure equilibration. In the extended theory, pores (including cracks) form multiple sets. Such sets are either weakly connected or isolated from each other, leading to non-uniform fluid content changes and fluid pressure changes within a bulk medium. Each set may induce anisotropy, meaning that pores in a set are not necessarily randomly oriented. Also, the solid matrix—in which the sets are embedded—is allowed to be anisotropic.

In Section 2, we have indicated practical scenarios pertinent to our extension and conceptual model: hierarchical porosity, complex porosity, and clustered porosity. Also, we referred to the cases where a simpler theoretical extension of isotropic dual porosity was already utilized with satisfactory results. In Section 3, we formulated the strain-stress relations that employed novel poroelastic coefficients a_{ij} and $b_{ij}^{(p)}$. In Section 4, we determined the physical meaning of these coefficients. a_{ij} can be viewed as storages under constant stress, whereas $b_{ij}^{(p)}$ are the poroelastic expansions or products of storages and Skempton-like coefficients. Several types of tests to obtain a_{ij} and $b_{ij}^{(p)}$ were proposed. In Section 5, we discussed alternative formulations of strain-stress relations. Alternative coefficients $1/M^{(p)}$ and $\alpha_{ij}^{(p)}$ were proposed and determined. $1/M^{(p)}$ can be viewed as storages under no frame deformation, whereas $\alpha_{ij}^{(p)}$ are the Biot-like coefficients. Relevant types of laboratory experiments were indicated. Finally, in Section 6, we introduced time dependency to obtain the governing equations of three-dimensional consolidation (39)–(40). To do so, we proposed the extended Darcy's law and fluid continuity equations. These equations were combined with mixed strain-stress formulations to obtain novel diffusion equations. The remaining governing equations were derived from the stress equilibrium conditions. In Section 7, the usage of consolidation equations was demonstrated on novel simulations of the triple-porosity case. These numerical examples demonstrated that the pore sets pressure evolution and interplay is controlled by the relative differences in permeability and poroelastic coefficients between pore sets. The simulations of the time-dependent drained behaviour of a multi-porous anisotropic poroelastic material show that positive pore pressure transients are generated in the weakly connected pore sets, and these could potentially be of sufficient magnitude and duration to push the material towards brittle failure.

NOMENCLATURE
Bulk medium perspective
Constant properties

$\Delta_{ijk\ell}$	effect of fluid in a medium
δ	shape factor inside leakage coefficient
μ	fluid viscosity
ν	Poisson's ratio of a drained medium
ν_s	Poisson's ratio of a solid phase
B_{ij}	Skempton coeff. of a medium
$C_{ijk\ell}$	drained elasticity tensor
$C^u_{ijk\ell}$	undrained elasticity tensor
E	Young's modulus of a drained medium
E_s	Young's modulus of a solid phase
K	bulk modulus of a drained medium
K_s	bulk modulus of a solid phase
L	fracture spacing
$S_{ijk\ell}$	drained compliance tensor
$S^u_{ijk\ell}$	undrained compliance tensor
S	fluid storage in a medium
V	volume of a medium

Variables

ζ	fluid content change in a single-porosity medium
ζ_{tot}	total fluid content change in a medium
ε_{ij}	strain tensor
σ_{ij}	stress tensor
p_c	change of confining pressure
p_f	change of fluid pressure
U_i	displacement of a fluid contained in a medium
u_i	displacement of a solid skeleton

Mesoscopic perspective
Constant properties

$\alpha^{(p)}_{ij}$	Biot-like coeff. of a p-th set
$\Gamma^{(p,q)}$	interset leakage between p-th and q-th sets
$\Delta^{(p)}_{ijk\ell}$	effect of fluid of a p-th set
$\nu^{(c)}$	Poisson's ratio of a drained constituent containing a set
$\phi^{(p)}$	volume fraction of a p-th set
$a_{p+1,p+1}$	constant-stress storage of a p-th set
$a_{p+1,q+1}$	constant-stress storage at sets' intersection
$b^{(p)}_{ij}$	expansion coeff. of a p-th set
$B^{(p)}_{ij}$	Skempton-like coeff. of a p-th set
$E^{(c)}$	Young's modulus of a drained constituent containing a set
$k^{(p)}_{ij}$	permeability coeff. of a p-th set
$M^{(p)}$	no-frame-deformation storage of a p-th set
$M^{(p,q)}$	no-frame-deformation storage at sets' intersection

$N^{(p)}$	relative storage of a p-th set
$N^{(p,q)}$	relative storage at sets' intersection
$S^{(p)}$	constant-stress storage of a p-th set
$S^{(p,q)}$	constant-stress storage at sets' intersection
$V^{(p)}$	volume of a set
$v^{(c)}$	volume fraction of a constituent containing a set

Variables

$\zeta^{(p)}$	external fluid increment to p-th set
$\zeta^{(p,q)}$	interset fluid increment between p-th and q-th sets
$p_f^{(p)}$	change of fluid pressure in p-th set
$q^{(p)}$	fluid flux to a p-th set
$U_i^{(p)}$	displacement of a fluid contained in a p-th set

CONFLICT OF INTEREST STATEMENT
The authors declare no conflicts of interest.

DATA AVAILABILITY STATEMENT
The codes used for the numerical simulations in Section 7 of this study are freely available at Adamus et al.[80] via https://doi.org/10.5281/zenodo.8001566.

The aforementioned codes are written as Matlab scripts and are contained in a folder named "triple-porosity". Our folder works as a module dependent on MRST; it must be integrated with this free open-source software available to download via https://www.sintef.no/projectweb/mrst/. See readme.txt inside the folder for more information.

ORCID
Filip P. Adamus https://orcid.org/0000-0002-4361-4104

REFERENCES
1. Biot MA. General theory of three-dimensional consolidation. *J Appl Phys*. 1941;12:155-164.
2. Biot MA. Theory of elasticity and consolidation for a porous anisotropic solid. *J Appl Phys*. 1955;26:182-185.
3. Biot MA. Theory of deformation of a porous viscoelastic anisotropic solid. *J Appl Phys*. 1956;27:459-467.
4. Biot MA. Theory of finite deformations of porous solids. *Indiana Univ Math J*. 1972;21:597-620.
5. Booker R, Savvidou C. Consolidation around a spherical heat source. *Int J Solids Struct*. 1984;20:1079-1090.
6. Sherwood JD. Biot poroelasticity of a chemically active shale. *Proc R Soc Lond A*. 1993;440:365-377.
7. Taron J, Elsworth D, Min KB. Numerical simulation of thermal-hydrologic-mechanical-chemical processes in deformable, fractured porous media. *Int J Rock Mech Min Sci*. 2009;46:842-854.
8. Cheng AH-D. *Poroelasticity*. 1st ed. Springer; 2016.

9. Aifantis E. Introducing a multi-porous medium. *Dev Mech*. 1977;8:209-211.

10. Aifantis E. Continuum theories of diffusion and infiltration. *Eng Sci Persp*. 1980a;5:10-20.

11. Aifantis E. *The mechanics of diffusion in solids*. TAM Report No 440, University of Illinois; 1980b.

12. Aifantis E. On the Problem of Diffusion in Solids. *Acta Mech*. 1980c;37:265-296.

13. Barenblatt GI, Zheltov IP, Kochina IN. Basic concepts in the theory of seepage of homogeneous liquids in fissured rocks [strata]. *J Appl Math Mech*. 1960;24:1286-1303.

14. Warren JE, Root PJ. The behavior of naturally fractured reservoirs. *Soc Pet Eng J*. 1963;228:245-255.

15. Elsworth D, Bai M. Flow-deformation response of dual-porosity media. *J Geotech Eng*. 1992;118:107-124.

16. Odeh AS. Unsteady-state behavior of naturally fractured reservoirs. *Soc Pet Eng J*. 1965;5:60-64.

17. Duguid JO, Lee PC. Flow in fractured porous media. *Water Resour Res*. 1977;13:558-566.

18. Ashworth M, Doster F. Foundations and their practical implications for the constitutive coefficients of poromechanical dual-continuum models. *Transp Porous Media*. 2019;130:699-730.

19. Wilson RK, Aifantis EC. On the theory of consolidation with double porosity. *Int J Eng Sci*. 1982;20:1009-1035.

20. Khaled MY, Beskos DE, Alfanlls EC. On the theory of consolidation with double porosity–III. A finite element formulation. *Int J Numer Anal Methods Geomech*. 1984;8:101-123.

21. Cho TF, Plesha ME, Haimson BC. Continuum modelling of jointed porous rock. *Int J Numer Anal Methods Geomech*. 1991;15:333-353.

22. Berryman JG, Wang HF. The elastic coefficients of double-porosity models for fluid transport in jointed rock. *J Geophys Res*. 1995;100:24611-24627.

23. Berryman JG, Pride SR. Models for computing geomechanical constants of double-porosity materials from the constituents' properties. *J Geophys Res*. 2002;107:1-14.

24. Berryman JG. Extension of poroelastic analysis to double-porosity materials: new technique in microgeomechanics. *J Eng Mech*. 2002;128:840-847.

25. Nguyen VX, Abousleiman YN. Poromechanics solutions to plane strain and axisymmetric mandel-type problems in dual-porosity and dual-permeability medium. *J Appl Mech*. 2010;77:1-18.

26. Mehrabian A, Abousleiman NA. Generalized Biot's theory and Mandel's problem of multiple-porosity and multiple-permeability poroelasticity. *J Geophys Res Solid Earth*. 2014;119:2745-2763.

27. Mehrabian A. The poroelastic constants of multiple-porosity solids. *Int J Eng Sci*. 2018;132:97-104.

28. Zhang Q, Borja RI. Poroelastic coefficients for anisotropic single and double porosity media. *Acta Geotech*. 2021;16:3013-3025.

29. Zhao Y, Borja RI. Poroelastic coefficients for anisotropic single and double porosity media. *Comput Methods Appl Mech Eng*. 2021;380:113797.

30. Zhang Q, Yan X, Shao J. Fluid flow through anisotropic and deformable double porosity media with ultra-low matrix permeability: a continuum framework. *J Pet Sci Eng*. 2021;200:108349.

31. Zhang Q, Yan X, Li Z. A mathematical framework for multiphase poromechanics in multiple porosity media. *Comput Geotech*. 2022;146:104728.

32. Zhang W, Mehrabian A. Coupled poromechanics and adsorption in multiple-porosity solids. *Phys Mesomech*. 2023;26:402-414.

33. Adamus FP, Healy D, Meredith PG, Mitchell TM. Multi-porous extension of anisotropic poroelasticity: linkage with micromechanics. *Int J Numer Anal Methods Geomech*. 2024:1-27. doi:10.1002/nag.3722

34. Halliwell CA, Dann SE, Ferrando-Soria J, et al. Hierarchical assembly of a micro- and macroporous hydrogen-bonded organic framework with tailored single-crystal size. *Angew Chem Int Ed*. 2022;61:e202208677.

35. Cowin SC, Gailani G, Benalla M. Hierarchical poroelasticity: movement of interstitial fluid between porosity levels in bones. *Phil Trans R Soc A*. 2009;367:3401-3444.

36. Wang G, Li P, Hao F, Zou H, Yu X. Dolomitization process and its implications for porosity development in dolostones: a case study from the lower Triassic Feixianguan Formation, Jiannan area, Eastern Sichuan Basin, China. *J Pet Sci Eng*. 2015;131:184-199.

37. Xu ZX, Li SY, Li BF, Chen DQ, Liu ZY, Li ZM. A review of development methods and EOR technologies for carbonate reservoirs. *Pet Sci*. 2020;17:990-1013.

38. Warren JK. *Evaporites. Their Evolution and Economics*. Blackwell Scientific Publications; 1999.

39. Thomson PR, Hazel A, Hier-Majumder S. The influence of microporous cements on the pore network geometry of natural sedimentary rocks. *Front Earth Sci*. 2019;7:1-14.

40. Bjørlykke K, Jahren J. Sandstones and sandstone reservoirs. In: *Petroleum Geoscience*. Springer; 2015.

41. Wu L, Li Y, Fu Z, Su BL. Hierarchically structured porous materials: synthesis strategies and applications in energy storage. *Natl Sci Rev*. 2020;7:1667-1701.

42. Carbajo J, Esquerdo-Lloret TV, Ramis J, Nadal-Gisbert AV, Denia FD. Acoustic modeling of perforated concrete using the dual porosity theory. *Appl Acoust*. 2017;115:150-157.

43. Bécot FX, Jaouen L, Gourdon E. Applications of the dual porosity theory to irregularly shaped porous materials. *Acta Acust United Acust*. 2008;94:715-724.

44. Liu X, Ma X, Yu C, Xin F. Sound absorption of porous materials perforated with holes having gradually varying radii. *Aerosp Sci Technol*. 2022;120:107229.

45. Lemonnier P, Bourbiaux B. Simulation of naturally fractured reservoirs. State of the art. Part 1. Physical mechanisms and simulator formulation. *Oil Gas Sci Technol*. 2010;65:239-262.

46. Karimi-Fard M, Gong B, Durlofsky LJ. Generation of coarse-scale continuum flow models from detailed fracture characterizations. *Water Resour Res*. 2006;42:1-13.

47. Luo Q, Yan Z, Yang Y, et al. Application of multilevel and high-resolution discrete fracture modeling based on unstructured grid in fractured reservoir simulation study. In: Lin J. eds *Proceedings of the International Field Exploration and Development Conference 2021*. IFEDC 2021. SSGG. Springer; 2022:28-37.

48. Huang Y, Liu J, Elsworth D, Leong YK. A transient dual porosity/permeability model for coal multiphysics. *Geomech Geophys Geo*. 2022;8:1-15.

49. Espinoza DN, Shovkun I, Makni O, Lenoir N. Natural and induced fractures in coal cores imaged through x-ray computed microtomography—impact on desorption time. *Int J Coal Geol*. 2016;154-155:165-175.

50. Mahzari P, Stanton-Yonge A, Sanchez-Roa C, et al. Characterizing fluid flow paths in the Hellisheidi geothermal field using detailed fault mapping and stress-dependent permeability. *Geothermics*. 2021;94:102-127.

51. Genter A, Traineau H. Hydrothermally altered and fractured granite as an HDR reservoir in the EPS-1 borehole, Alsace, France. *Proc 17th Workshop Geotherm Reserv Eng, Stanford University*. 1992:33-38.

52. Heidsiek M, Butscher C, Blum P, Fisher C. Small-scale diagenetic facies heterogeneity controls porosity and permeability pattern in reservoir sandstones. *Environ Earth Sci*. 2020;79:1-14.

53. Brantut N, Aben FM. Fluid pressure heterogeneity during fluid flow in rocks: new laboratory measurement device and method. *Geophys J Int*. 2021;225:968-983.

54. Farrell NJC, Healy D, Taylor CW. Anisotropy of permeability in faulted porous sandstones. *J Struct Geol*. 2014;63:50-67.

55. Rizzo RE, Healy D, Heap MJ, Farrell NJ. Detecting the onset of strain localization using two-dimensional wavelet analysis on sandstone deformed at different effective pressures. *J Geophys Res Solid Earth*. 2018;123:460-478.

56. Panwar DS, Saxena VK, Chaurasia RC, Singh AK. Prospective evaluation of coal bed methane in Raniganj coal field, India. *Energy Sources A: Recovery Util Environ Eff*. 2017;39:946-954.

57. Paterson M, Wong TF. *Experimental Rock Deformation—The Brittle Field*. 2nd ed. Springer; 2005.

58. Rutter E, Mecklenburgh J, Bashir Y. Matrix gas flow through "impermeable" rocks—shales and tight sandstone. *Solid Earth*. 2022;13:725-743.

59. Leclère H, Faulkner D, Wheeler J, Mariani E. Permeability control on transient slip weakening during gypsum dehydration: implications for earthquakes in subduction zones. *EPSL*. 2016;442:1-12.

60. Baud P, Meredith P, Townend E. Permeability evolution during triaxial compaction of an anisotropic porous sandstone. *J Geophys Res Solid Earth*. 2012;117:1-23.

61. Biot MA. Mechanics of deformation and acoustic propagation in porous media. *J Appl Phys*. 1962;33:1482-1498.

62. Berryman JG, Wang HF. Elastic wave propagation and attenuation in a double-porosity dual-permeability medium. *Int J Rock Mech Min Sci*. 2000;37:63-78.

63. Brantut N. Dilatancy-induced fluid pressure drop during dynamic rupture: direct experimental evidence and consequences for earthquake dynamics. *EPSL*. 2020;538:116179.

64. Elsigood B, Brantut N, Meredith PG, Healy D, Mitchell TM, Aben FM. Stress-induced anisotropic poroelasticity in westerly granite. *J Geoph Res: Solid Earth*. 2023;128:e2023JB026909.

65. Liu D, Brantut N, Aben FM. Opposite variations for pore pressure on and off the fault during simulated earthquakes in the laboratory. arXiv. 2401.14506 2024:1-30.

66. Adamus FP, Stanton-Yonge A, Mitchell TM, Healy D, Meredith PG. Uniaxial compression of 3D printed samples with voids: laboratory measurements compared with predictions from effective medium theory. arXiv. 2310.13956 2023:1-43.

67. Cheng AHD. Material coefficients of anisotropic poroelasticity. *Int J Rock Mech Min Sci*. 1997;34:199-205.

68. Biot MA. Thermoelasticity and irreversible thermodynamics. *J Appl Phys*. 1956;27:240-253.

69. Borja RI, Koliji A. On the effective stress in unsaturated porous continua with double porosity. *J Mech Phys Solids*. 2009;57:1182-1193.

70. Lie KA, Møyner O, eds. *Advanced Modelling with the MATLAB Reservoir Simulation Toolbox*. Cambridge University Press; 2021.

71. Ashworth M, Doster F. An open source numerical framework for dual-continuum geomechanical simulation. *SPE RSC*. 2019:1-20.

72. Mehrabian A, Abousleiman YN. Theory and analytical solution to Cryer's problem of N-porosity and N-permeability poroelasticity. *J Mech Phys Solids*. 2018;27:218-227.

73. Zhang S, Liu J, Wei M, Elsworth D. Coal permeability maps under the influence of multiple coupled processes. *Int J Coal Geol*. 2018;187:71-82.

74. Pabst W, Gregorová E. Young's modulus of isotropic porous materials with spheroidal pores. *J Eur Ceram*. 2014;34:3195-3207.

75. Lutz MP, Zimmerman RW. The effect of pore shape on the poisson ratio of porous materials. *Math Mech Solids*. 2021;26:1191-1203.

76. Selvadurai AP, Suvorov AP. The influence of the pore shape on the bulk modulus and the Biot coefficient of fluid-saturated porous rocks. *Sci Rep*. 2020;10:18959.

77. Lockner DA. Rock Failure. In: Ahrens TJ. ed. *Rock Physics & Phase Relations*. 1995;3:127-147.

78. Berryman JG. Effective medium theories for multicomponent poroelastic composites. *J Eng Mech*. 2006;132:519-531.

79. Berkowitz B. Characterizing flow and transport in fractured geological media: a review. *Adv Water Reour*. 2002;25:861-884.
80. Adamus FP, Healy D, Meredith PG, Mitchell TM, Stanton-Yonge A. multi-porous extension of anisotropic poroelasticity: consolidation and related coefficients [Dataset]. *Zenodo*. 2023. doi:10.5281/zenodo.8001566

APPENDIX: STRESS-STRAIN RELATIONS FOR DUAL POROSITY

Herein, we rewrite Equations (24)-(25) to obtain stress-strain relations for dual porosity. We get

$$\sigma_{ij} = \sum_{k=1}^{3} \sum_{\ell=1}^{3} \left(C_{ijk\ell}^{u} - 2N^{(1,2)}\alpha_{ij}^{(1)}\alpha_{k\ell}^{(2)} \right) e_{k\ell} + \left(N^{(1,2)}\alpha_{ij}^{(2)} - N^{(1)}\alpha_{ij}^{(1)} \right)\zeta^{(1)} + \left(N^{(1,2)}\alpha_{ij}^{(1)} - N^{(2)}\alpha_{ij}^{(2)} \right)\zeta^{(2)},$$

$$p_{f}^{(1)} = \sum_{k=1}^{3} \sum_{\ell=1}^{3} \left(N^{(1,2)}\alpha_{k\ell}^{(2)} - N^{(1)}\alpha_{k\ell}^{(1)} \right) e_{k\ell} + N^{(1)}\zeta^{(1)} - N^{(1,2)}\zeta^{(2)},$$

$$p_{f}^{(2)} = \sum_{k=1}^{3} \sum_{\ell=1}^{3} \left(N^{(1,2)}\alpha_{k\ell}^{(1)} - N^{(2)}\alpha_{k\ell}^{(2)} \right) e_{k\ell} + N^{(2)}\zeta^{(2)} - N^{(1,2)}\zeta^{(1)},$$

where

$$N^{(1)} := \frac{M^{(1)}M^{(1,2)}M^{(1,2)}}{M^{(1,2)}M^{(1,2)} - M^{(1)}M^{(2)}},$$

$$N^{(2)} := \frac{M^{(2)}M^{(1,2)}M^{(1,2)}}{M^{(1,2)}M^{(1,2)} - M^{(1)}M^{(2)}},$$

$$N^{(1,2)} := \frac{M^{(1)}M^{(2)}M^{(1,2)}}{M^{(1,2)}M^{(1,2)} - M^{(1)}M^{(2)}}$$

are the coefficients described by the combinations of storages. If the two sets are isolated from each other, then $1/M^{(1,2)} = 0$. In such a case $N^{(1)} = M^{(1)}$, $N^{(2)} = M^{(2)}$, $N^{(1,2)} = 0$ and the above stress-strain relations reduce to (28)-(29), as expected.